Atomic Layer Deposition (ALD) Assisting the Visibility of Metal-organic Frameworks (MOFs) Technologies

Jianwei Ren*, Tien-Chien Jen

University of Johannesburg, Johannesburg, Kingsway and University Road, Auckland Park, 2092, P.O. Box 524, Auckland Park, 2006, Johannesburg, South Africa

Corresponding author. Tel: +27 11 559 2103. Email: jren@uj.ac.za (J. Ren)

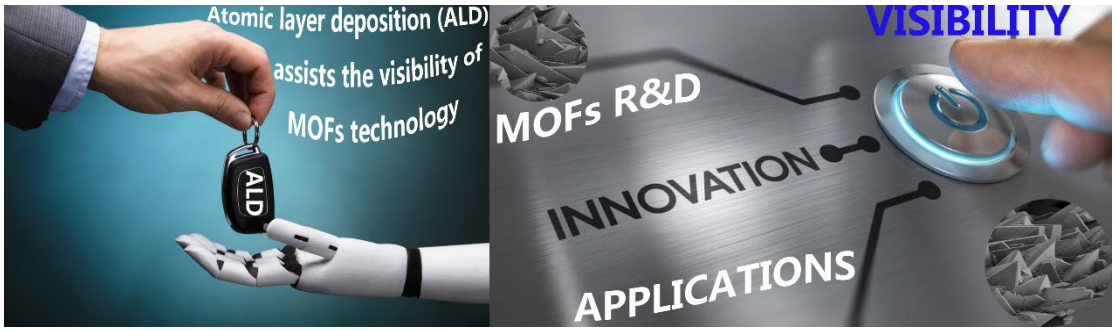

Abstract

Metal-organic frameworks (MOFs) materials have been thought to be magic powers with unlimited applications. However, their powdered condition presents difficulty in utilizing them widely in practices. Depending on the envisioned applications, MOFs will be desired to integrate as an application-oriented forms for example thin films into a microelectronic device to achieve the desired performance. In the last decades, atomic layer deposition (ALD) as a truly enabling technology has become the method of choice for films deposition with good quality-control. In this regard, ALD promises to deposit MOFs films onto the target substrates and assist the visibility of MOFs technologies by facilitating MOFs devices integration. This review will collect together the published work that addresses the past ALD research efforts towards MOFs devices integration. Meanwhile, some beneficial concepts from other technological matrix are also pulled in to sparkle the thinking. We aim to provide an understanding on how the ALD technique is currently assisting the visibility of MOFs technologies.

Keywords: Atomic layer deposition; Metal-organic frameworks; Technology readiness levels; Visibility of MOFs technologies

Contents

List of abbreviations

A

AFM: Atomic force microscopy

AIM: ALD in MOFs

ALD: Atomic layer deposition

Al_2O_3: Aluminium oxide

AP-SALD: Atmospheric pressure

B

BET: Brunauer-Emmett-Teller

BN: Boron nitride

BTC: 1,3,5-benzenetricarboxylic

β-CD: βcyclodextrin

C

CEES: 2-chloroethyl ethyl sulphide

CTAB: Cetyltrimethylammonium bromide

CVD: Chemical vapor deposition

CVR: Chemical vapor reaction

CWAs: Chemical warfare agents

D

DED: Difference envelope density

DMF: dimethylformamide

DFT: Density functional theory

DMNP: Dimethyl 4-nitrophenyl phosphate

DRIFT: Diffuse reflectance infrared Fourier transform

E

EDS: Energy dispersive X-ray spectroscopy

EG: Ethylene glycol

F

FBR: Fluidized bed reactor

Fe_2O_3: Iron oxide

FTIR: Fourier-transform infrared

FTO: Fluorine-doped tin oxide

G

GC-MS: Gas chromatograph coupled with mass selective detector

GIWAXS: Grazing Incidence Wide Angle X-ray Scattering

GPC: Growth-per-cycle

H

H_2BDC: Terephthalic acid

H_3BTC: Trimeric acid

HAADF: High-angle annular dark-field

HDS: Hydroxy double salt

HKUST: Hong Kong University of Science and Technology

HKUST-1: $Cu_3(BTC)_2(H_2O)_3$; BTC^{3-}=benzene-1,3,5-tricarboxylate

H_2TCPP: 5,10,15,20-tetrakis(4-carboxyphenyl)porphyrin

H_4TCPP: 4,4',4'',4'''- (porphyrin-5,10,15,20-tetrayl) tetrabenzoic acid

HRTEM: High-resolution transmission electron microscopy

I

ICP-OES: Inductively coupled plasma-optical emission spectroscopy

L

LBL: Layer-by-layer

LMGP: Laboratory of Materials and Physical Engineering

LPE: Layer-by-layer liquid-phase epitaxy

M

ME: Metal exchange

$MeCpPtMe_3$: Methylcyclopentadienyl-trimethyl platinum

MIL: Matérial Institut Lavoisier

MLD: Molecular layer deposition

MOFs: Metal-organic frameworks

MTBC: Methanetetrakis *p*-biphenylcarboxylate

N

NCs: nanocrystals

NMR: Nuclear magnetic resonance

NPs: nanoparticles

NU: Northwestern University

O

1,4-BDC: 1,4-benzenedicarboxylic acid

P

PA-6: Polyamide-6 nanofiber

PDF: Pair distribution function

PDMS: Polydimethylsiloxane

PEN: Polyethylene naphthalate

PP: Polypropylene

PXRD: Powder X-ray diffraction

Q

QCM: Quartz crystal microbalance

QMS: Quadrupole mass spectrometer

R

RD&I: Research, development and innovation

RPM: Rounds per minutes

S

SAED: Selected-area electron diffraction

SALD: Spatial atomic layer deposition

SALI: Solvent-assisted ligand incorporation

SAMs: Self-assembled monolayers

SBUs: Secondary building units

SCCM: Standard cubic centimeters per minute

SEM: Scanning electron microscope

$Si(OMe)_4$: Tetramethoxysilane

SiO_2: Silicon dioxide

SHE: Safety, health and environment

SIM: Solvothermal deposition in MOFs

SPME: Solid phase microextraction

STEM: Scanning transmission electron microscopy

STY: Space-time-yield

T

2D: Two-dimensional

3D: Three-dimensional

TOF: Turnover frequency

TEM: Transmission electron microscopy

TGA: Thermogravimetric analyses

$TiCl_4$: Titanium tetrachloride

TiO_2: Titanium dioxide

TMA: Trimethylaluminum

TRLs: Technology readiness levels

U

UiO: Universitetet i Oslo

UiO-66: $Zr_6O_4(OH)_4(BDC)_6$; BDC^{2-}=terephthalic acid

X

XAFS: X-ray absorption fine structure

XANES: X-ray absorption near edge structure

XAS: X-ray absorption spectroscopy

XPS: X-ray photo-electron spectroscopy

XRF: X-ray fluorescence

XRR: X-ray reflectivity

XAS: X-ray absorption spectroscopy

Z

ZIF: Zeolitic Imidazolate Framework

ZIF-8: $Zn(Melm)_2$; $Melm^-$=2-methylimidazolate

$ZnAc_2$: Zinc acetate

1. Introduction

1.1. Metal-organic Frameworks (MOFs) technologies

After 20 years of research and development, metal-organic frameworks (MOFs) are gradually coming out of the laboratories to solve real-world problems. As usual, there are always challenges need to be solved in order to integrate the laboratory-derived pieces into commercial devices, and the progression towards higher technology readiness levels (TRLs) needs the collective advancements from other available technologies.

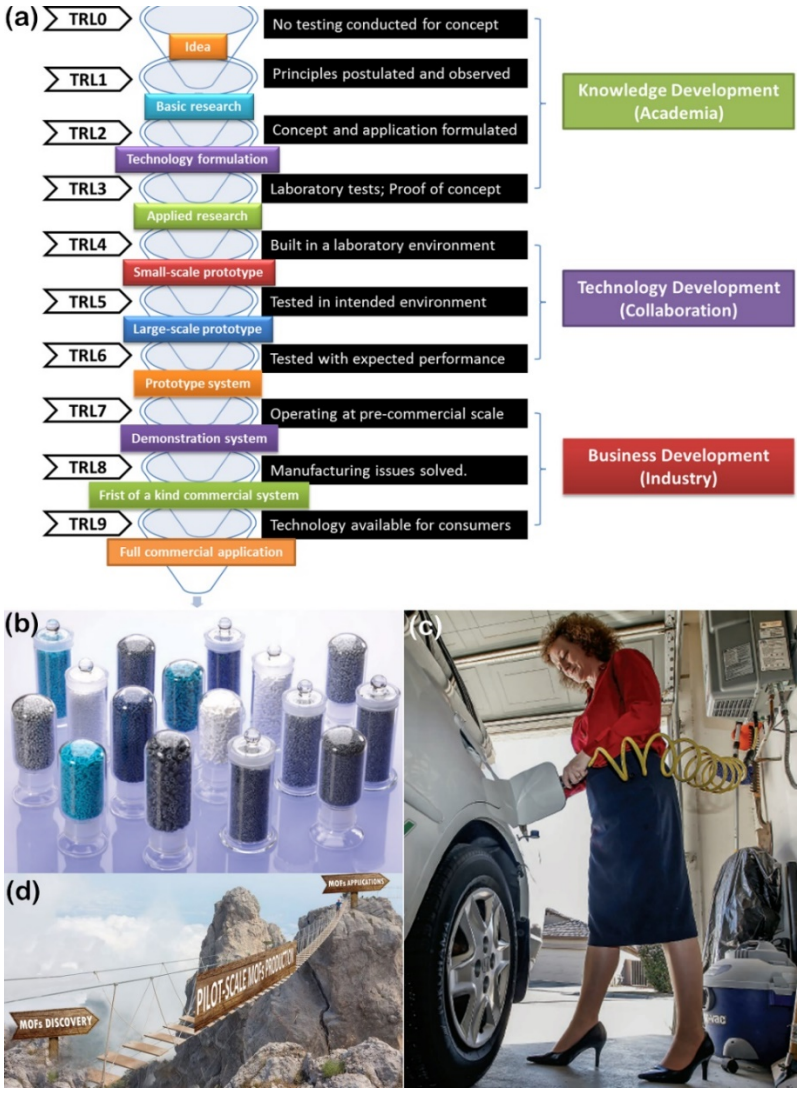

Figure 1. (a) The commonly defined technology readiness levels (TRLs). (b) Shaped bodies from different MOF materials. Reprinted with permissions [1], Copyright © Royal Society of Chemistry 2009. (c) Home refuelling and MOFs-integrated low-pressure tanks to be major game changers for natural gas-powered vehicle. Reprinted with permissions [2], Copyright © 2014 American Association for the Advancement of Science. (d) Pilot-scale production of cost-effective MOFs presented an example knowledge gap between MOFs discovery and applications. Reprinted with permissions [3], Copyright © 2017 Elsevier B.V.

Referring to the common definition of TRLs from level 0 to level 9 that illustrated in Figure 1a, the up-to-date MOFs research, development, and innovation (RD&I) are still sitting between TRL3 and TRL4. Classically, most of the RD&I activities on MOF materials have been concentrated in their applications as solid-state sorbent materials with some small-scale MOFs-enabled prototypes demonstrated worldwide. Since MOFs are usually derived as powder form from the laboratory synthesis, and for the ease of handling and further system integration purposes, powdered MOFs materials are often to be shaped into various application-oriented structures (Figure 1b). Figure 1c demonstrated MOFs-integrated tanks as an example to store natural gas at low-pressure for the natural gas-powered cars. Compared to the current-standard high-pressure cylinders up to 70 MPa working pressure, the adsorptive feature of the MOFs-integrated storage provided the possibility to store gas fuels at a medium pressure around 15 Mpa with much less risks. However, those prototypes will still take a while to go into the market, and the pilot-scale production of the cost-effective MOFs has been exampled as one of the knowledge gaps between MOFs discovery and applications (Figure 1d).

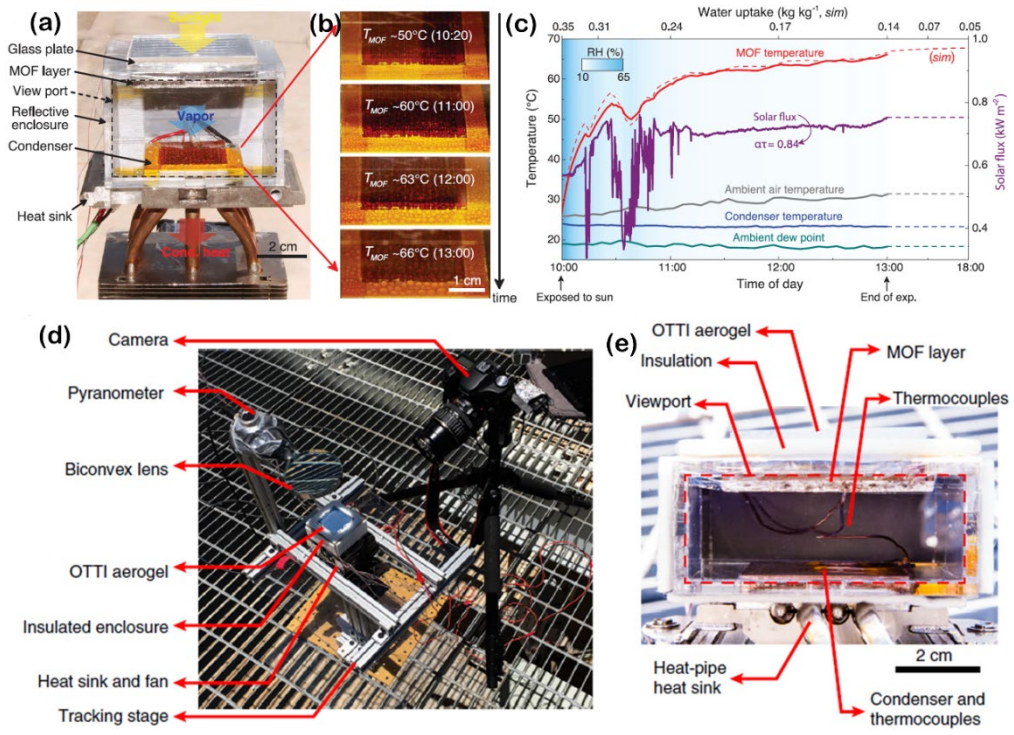

Figure 2. Outdoor water-harvesting prototype on MOF-801: (a,b) MOF-801 (1.34 g with a packing porosity of 0.85) integrated-prototype with outer dimensions of 7 cm (L) × 7 cm (W)× 4.5 cm (H). (c) Absorbed water changed with ambient temperatures. Reprinted with permissions [5]. Copyright © 2017, American Association for the Advancement of Science. (d) Testing apparatus of the water harvesting device. (e) MOF-801 integrated water-harvesting device (5 cm × 5 cm base × 2.57 mm thickness at packing porosity of 0.67). Reprinted with permissions [6]. Copyright © 2020 Springer Nature Limited.

MOFs in another exciting project from Yaghi group shown in Figure 2 was employed to collect the atmospheric water at ambient conditions, and no external power sources were required. Such success has provided a viable concept to supply with drinking-quality water in dry regions. After the laboratory tests were done by Trapani et al. [4] under meteorological simulations, Kim and his colleagues [5] reported in Science on the development of a water-harvesting prototype. The proof-of-concept was demonstrated outdoors with outer dimensions: 7 cm × 7 cm × 4.5 cm, and 1.34 g activated MOF-801 were packed at a porosity of 0.85 (Figure 2a,b). As reported (Figure 2c), the device was able to harvest water from ambient air by using low-grade heat directly from sunlight and 1 kg of MOF-801 could capture 2.8 L of H_2O daily at a relative humidity of 20%. Later, the same group [6] provided more detailed information on their test apparatus utilized in the course of the development of the water harvesting device. As illustrated in Figure 2d, a camera, a pyranometer, a heat sink and fan were installed on a tracking stage to serve the purpose. The MOFs-integrated H_2O-harvesting device in Figure 2e was equipped with a 5 cm × 5 cm device base, a 2.57 mm-thick MOF layer at packing porosity of 0.67, a condenser (4 cm × 4 cm), as well as several thermocouples.

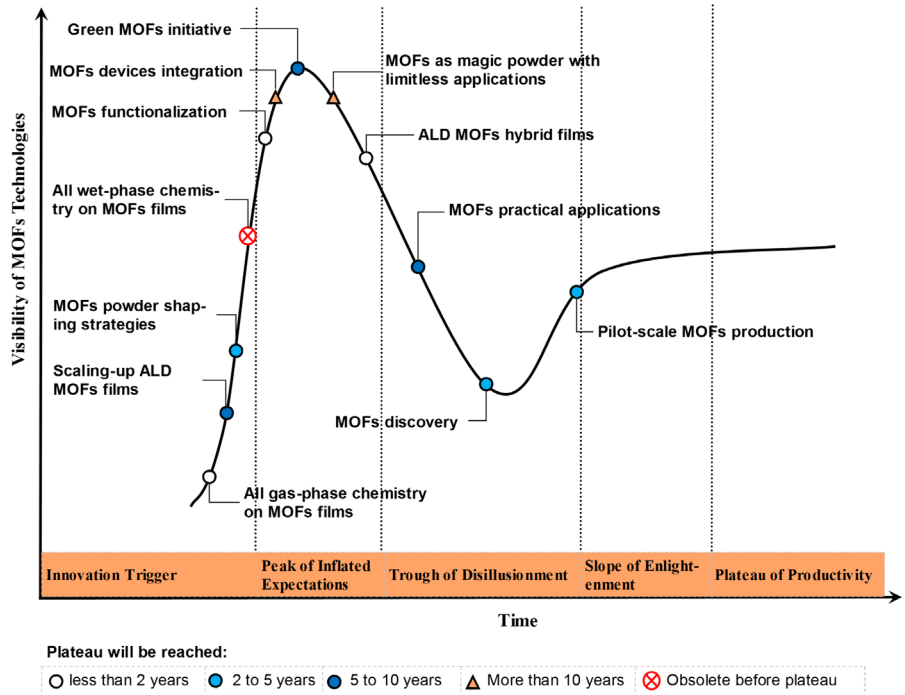

Plateau will be reached:

○ less than 2 years ● 2 to 5 years ● 5 to 10 years △ More than 10 years ⊗ Obsolete before plateau

Innovation trigger	In this stage, a technology is conceptualized. There may be prototypes, but frequently there are no functional products or market studies. The potential stimulates the interest of the communications media and, at times, demonstrations for testing the concept.
Peak of inflated expectations	The technology is implemented, especially by the early adopters. There is a lot of publicity about successful and unsuccessful implementations.
Trough of disillusionment	Defects and failures lead to certain disappointment with the technology. Some suppliers are unsuccessful or discard their products. Certain successful applications continue on their path.
Slope of enlightenment	There is a broader understanding of the technology's potential for new applications. More frequently the companies implement or test it in their environments. Some producers create further generations of products.
Plateau of productivity	The technology becomes widely implemented. Its place in the market and its applications are well-understood. Standards arise to evaluate technology providers.

Figure 3. Hype cycle for visibility of MOFs technologies and RD&I activities.

Certainly, despite the already-achieved excellence from the MOF-801-integrated water-harvesting prototype, to push this technology from TRL4 up to TRL7, there are some further considerations need to be taken care of, such as the hydro-stability of the chosen MOF material for H_2O-harvesting in air, the consumability of the produced H_2O by the device, technic-economic assessments of the device, additional device-engineering costs to allow this device viable for supplying drinking-quality water in the designated area, and so on. To address those issues, the collective efforts are necessary from an extensive multidisciplinary professions and specializations, for example, some pretty critical comments published in Science as 'Technical Comment' were made by Meunier [7] to recommend a modification on the process design to harvest H_2O in a continuous manner and also use of more suitable MOFs to achieve the set goals. Queen [8] raised certain thoughts towards the utilization of MOFs to pull water out of thin air, and pointed out the success of this technology would also pave the way of developing new systems for heating and cooling. Kalmutzki et al. [9] also proposed the strategies to fine-tune the adsorption behavior of the chosen MOFs through reticular chemistry and design for the next-generation MOFs for applications in passive adsorption-based H_2O-harvesting devices. Similar to other technologies, the RD&I activities of MOFs will also follow the general hype cycle curve, as illustrated in Figure 3. For instance, the intensive MOFs devices integration is sitting at the stage of 'Peak of Inflated Expectations', which indicates that the technology has been implemented by the early adopters, and there are attentions about successful and unsuccessful implementations. No matter what will be the ultimate MOFs-enabled applications, MOFs in the end always need to be compatible with their three-dimensional (3D) surroundings as well as the existing processing technologies. In other words, the visibility of MOFs technologies at the same time is subject to the availabilities of the other advancements such as the pilot-scale production of cost-effective MOFs, functionalization of MOFs, and MOFs power integration strategies. Besides, the development of synthetic strategies for green MOF materials featured with less-toxic meter centres and biomass-derived linkers has become another important promoter for MOF device integration.

1.2. Atomic layer deposition (ALD) technologies

In the past 30+ years, the RD&I activities around ALD have attracted extensive attention worldwide. ALD as a gas-phase technique was designed to coat thin films of numerous materials onto any target substrates. Relying on self-limiting surface chemistry and sequential reactions, ALD produced films with excellent controls on film thickness, composition, conformity, very low pin-hole and particle levels on planar substrates even on the high-aspect-ratio structures. Featured with these merits, ALD technique has been using worldwide as a reliable tool to coat films or fabricate membranes in different fields of applications [10]. Figure 4 illustrated how to achieve the desired thickness differently by several thin-film depositing

approaches. A continuous process (Figure 4a) would continue to operate the same process until the set time reached. A pulsed process (Figure 4b) as a flux-controlled process would repeat the cycles to achieve the desired thickness. In contrast, a surface-controlled ALD process (Figure 4c) based on self-limiting surface chemistry was able to achieve a fixed film thickness in each cycle, and more precise control on film thickness could be realized by running the right cyclic numbers. In other words, a cyclic ALD film with a fixed thickness would keep adding one atomic layer on the top of another, and all the cycles together contributed to the total film growth. More importantly, varying interactive films with different compositions could be realized by the repetition of dosing different precursors. Obviously, the surface chemistry based on self-limiting was the main mechanism for ALD to achieve its outstanding conformality and uniformity [11].

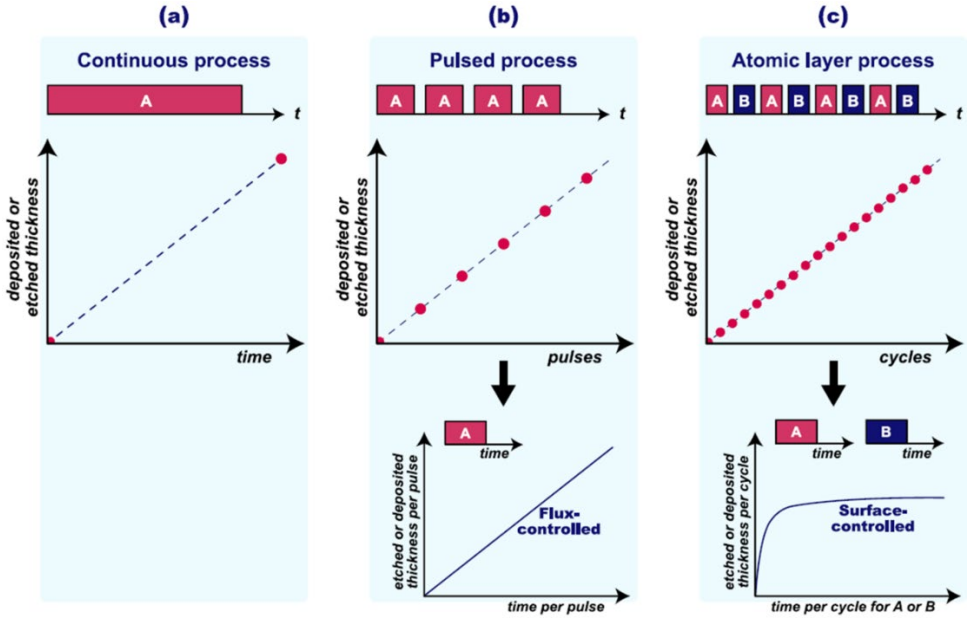

Figure 4. The comparison of several approaches for depositing thin films: (a) a continuous process to stop when the desired thickness reached. (b) a flux-controlled pulsed process repeated until the desired thickness reached. (c) a surface-controlled ALD cycle achieved fixed film thickness by repeating the right cycling numbers. Reprinted with permission [11]. Copyright © 2015, IOP Publishing.

For interests, Puurunen [12] gave a short but detailed story of ALD development since its first international patent on November 29, 1974, and Alvaro et al. [13] explained the evolution of ALD advancements. After the commercial onset of ALD, surface chemistries, and processes around ALD precursors as the enablers to grow the envisioned set of materials have been dedicated by the pioneering work [14–22]. Very often, ALD is chosen to meet the needs for coating films on 3D nanostructured surfaces, where the conformity of ALD films is a key indicator to judge the quality of the work. The status of knowledge about the conformity in ALD was reviewed by Cremers and co-workers [23]. Other ALD configurations had been

developed with similar characteristics and working principles [24,25]. All those developments have marketed ALD as a currently available technique to create uniform and conformal films at an atomic-scale accuracy. Following these waves, ALD has been continually extended for material functionalization or structures engineering in various fields like membrane technology, solar energy conversion, energy storage, catalysis, drug delivery, microelectronics [26–30]. Despite the progress that has been made so far, there have been consistent interests regarding how ALD as a high-tech tool would assist with the device integration of chosen materials such as deposition inorganic thin films on 3D polymer nanonetworks [31,32] or coating of carbon-nanostructures [33,34].

To date, there are various industrial and scientific scenarios with necessities to coat films of the interested materials on the surfaces of fine powder particles to obtain the designed surface functionalization. Compared to sol-gel techniques [35] and chemical vapor deposition (CVD) [36], ALD offers an ideal platform technology to assist with the particle coating technologies. Technically, any external or internal surfaces of the porous particles with active sites tending to absorb precursor molecules could be handled by ALD coating process [37]. In a recent review work done by Oviroh et al. [38], different types of film deposition technologies were compared in the aspects of advantages and disadvantages and the authors highlighted how ALD technologies expanded into nanotechnology areas. The purposeful thinking was that ALD could be adopted as a tool for nanotechnology with excellent conformity, low-temperature deposition, reliable thickness control and adjustable composition, and ALD coatings be applied as an effective approach to achieve the surface engineering of nanoparticles [39]. As summarized in Figure 5, practices on ALD have successfully been applied to 56 out of 118 elements on the periodic table for self-limiting films on nanoparticles.

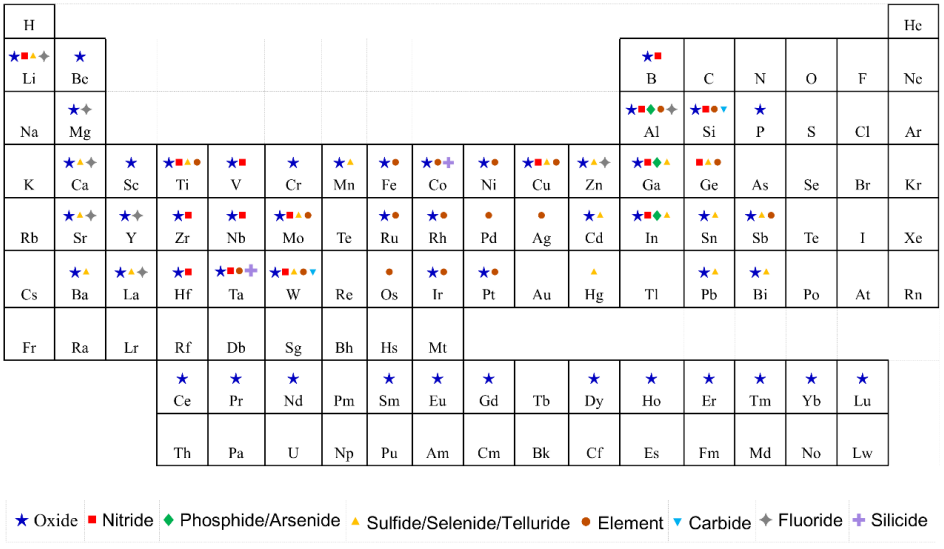

Figure 5. Periodic elements that have been succeeded in making ALD thin-films [40].

Generally, the ALD was understood to be easily applicable to the surface structure of the planar substrates, but for powder substrates with complex pore architecture and surface chemistry presented some challenges [41,42]. There were different desires and purposes for ALD on powder substrates, for instance, ALD coating to protect powder particles from oxidation or insulate them from electrical conduction. Apparently, those desires fit well into the scope that the optical, mechanical, or chemical properties of the powder particles could be tuned by ALD through coating films on the surface or fabricating hybrid structures. It was noted that not only ALD on powder substrates would be subjected to the capability of ALD to coat quality films on their high-aspect-ratio structures, but also the particle sizes and shapes as a coating bed would also have impacts to the quality of the ALD films. Furthermore, depending on whether the reactions occurred on the surface or inside the powder particles, new compounds or layer structures could be derived from the different diffusion rates or segregation of precursor molecules.

In literature, the most matured approach for ALD coating on powder substrates took place in a static bed, in which the precursor vapors diffused to reach all surfaces and then formed the coatings. As seen in Figure 6a, the bed could be in a powder tray or in a flow tube with specifically designed heating stage protocols. The diffusion kinetics for this type of reactor configuration might be simplified to a model by treating the bed as a series of channels between powder particles [43]. Some research groups have pioneered this area, for instance, Boron nitride (BN) nanoparticles were coated with silicon dioxide (SiO_2) films by Ferguson et al. [44] using such common ALD from $SiCl_4$ and H_2O, and in-situ FTIR was employed as the surface analysis technique. Later, a fluidized bed reactor (FBR) was introduced by the same group, which provided an option to scale-up the ALD process of coating nanoparticles [45]. It has been noted that although the ALD deposition of films on nanoparticle surfaces could occur in different reactor configurations, the FBR as illustrated in Figure 6b has been predominantly used for powder substrates due to the high efficient vapor-solids contacting efficiencies caused by their intense physical mixing [46], and the in-depth discussion of the ALD-FBR can be found elsewhere [47]. Usually, all ALD-FBRs have been incorporated with different measures to avoid powder particles from agglomerating in the ALD coating operations.

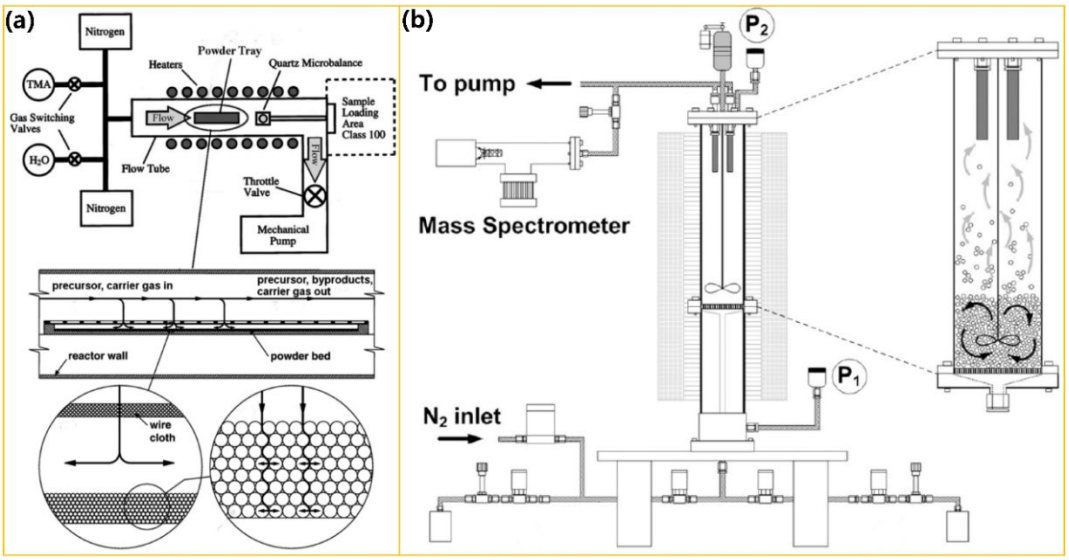

Figure 6. (a) Schematic of the common ALD reactor. Reprinted with permission [43]. Copyright © 2015 American Chemical Society. (b) FBR-integrated with real-time mass spectrometry for ALD on particles. Reprinted with permission [47]. Copyright © 2007 Elsevier B.V.

More recently, research efforts on ALD have been extended from graphene-kind powder materials to functionalize MOFs structures [48,49]. Given that MOFs materials are the new generation of materials with many potential applications, ALD in MOFs (AIM) offered new routes to modify MOFs materials with the designed functionalities, tune their surface chemical properties, or improve their catalysis performance. It was very often that the intrinsic properties of MOFs were expected to remain while creating ALD interactive films. Compared to graphene-kind powder materials, the more complex surface chemistry and the large aspect-ratios MOF pores were assumed to present difficulties in ALD practices. The influence of different MOF structures on their ALD processes need to be probed before functionalizing the target MOF surfaces and any further device integrations.

This work will review the past RD&I efforts and practical activities relevant to ALD-MOFs to provide understanding on how the ALD technique has been assisting the visibility of MOFs technologies. The fundamental strategies of ALD as a tool for MOFs-integrated devices will be focused by starting with an introduction of several essential advancements of importance for MOFs devices integration, including (i) MOFs surface preparation and defect engineering, (ii) suitable MOFs pore sizes, (iii) all gas-phase techniques for depositing MOFs films, (iv) ALD MOF films scaling-up solutions. (v) essential characterization techniques for ALD MOFs films, and (vi) toxicity evaluation on ALD MOFs device integration. Then, the relevant practices on ALD-MOFs towards MOFs devices integrations are reviewed covering ALD post-synthetic functionalization of MOFs, ALD confinement of nano-catalysts into MOFs, ALD deposition of MOFs films on target substrates and theoretical studies. In the context, the parallel

advancements such as lessons or concepts from other technologies to be beneficial are also drawn to guide further optimization and improvement of applications based on MOFs-enabled technologies. Lastly, the summary and the future perspective are given.

2. Important advancements for ALD-MOFs device integration

2.1. MOFs surface preparation and defect engineering

Although ALD commits to coat functional films by design on the target substrates, the availability of reactive sites on the surfaces of substrates are crucial for the precursor molecules to adsorb effectively. In other words, ALD films deposition on a MOF substrate with perfect structure can pose a challenge for the chemisorption of the precursor molecules, as a result, ALD on defect-free MOF surfaces likely yields poor film coverage, and this is not favorable by any further MOFs device integration. Therefore, the surface preparation is necessary to create functional groups on the MOFs surfaces, which can normally be achieved by a pre-deposited seeding-layer or creation of structural defects on the MOFs surfaces. Indeed, MOF structural defects has been recognized to change MOF's textural properties and chemical behaviors [50−53]. Of course, the optimization of the ALD process conditions will be always the first choice to achieve the best precursor coverage on the MOFs surfaces, for instance to find the optimized deposition temperature, select a better precursor, and set the right cyclic times. Defect engineering in the MOF structures will be another important solution to facilitate the ALD process, and the concentration of defects needs to be controlled toward applications of interests. It's noted that MOFs synthesized from straightforward routes tended to display inherent defects, unless specific cautions and measurements were taken during the synthesis process. The defects usually presented as dangling linkers, missing metal centres, dislocations, misconnections, or interwoven during the crystallization process [54]. Bear the above in mind, the MOFs synthesizing routes and reaction conditions are of importance to provide the possibilities of controlling the formation and concentration of MOFs structural defects. In fact, 'Defects engineering' in MOFs has been proved to be an important strategy to tune their physical and chemical behaviors [55,56]. The lack of such control will hinder the formation of compositional MOF gradients on the targeting substrates, and subsequently limit the rational design of MOF structural defects for the envisioned applications [57,58]. In this regard, one of the liquid phase approaches called 'in-flow MOF lithography' has demonstrated the accomplishment of controlling MOF gradients towards MOF defect engineering, where the diffusion of MOF precursors were controlled inside the designed microfluidic channels to enable the spatiotemporal control during the generation of MOF thin films [59]. For the

interests of ALD-MOFs, the concept of 'defects engineering' can be a way to tailor the structural properties of a given MOF substrate so as to facilitate the chemisorption of the precursor molecules into its structure.

2.2. Suitable MOF pore sizes to facilitate the diffusion of ALD precursors

As understood from the literature that one of the critical encountered issues for ALD in porous materials was the slow diffusion rate of the chemical precursors into small pores [60–62]. Given the nanosized pores in MOFs structures, the inefficient diffusion of precursors would pose an actual constraint for the ALD process to deliver perfect film coverages and high production rates. One straightforward way of mitigating these problems is to select or synthesize MOFs with ideal pore sizes to diffuse the used ALD precursors efficiently. For example, MOF NU-1000(Zr) with ~3 nm hexagonal channels were selected by Hupp and co-workers for ALD incorporation of catalytically actives, i.e. Al^{3+}, Zn^{2+} and cobalt sulfide [63,64]. The mechanism on the interaction between ALD precursors and MOF nodes was probed by computational studies [65]. Similarly, the ALD of NiO was demonstrated by Jeong et al [66] into the studied MIL-101(Cr) MOF framework consisted of two types of pores between 2.5–3.5 nm. However, the Cr-nodes of MIL-101(Cr) MOF were found to bind with H_2O molecules, which prevented the efficient diffusion of ALD precursor molecules [67]. Luckily, these coordinated H_2O molecules had been demonstrated by Huang et al. [68] in the earlier work to be easily removable by applying heat treatment under vacuum at 150 °C. More importantly, the resulting coordinatively unsaturated sites became readily active to improve the diffusion rate of precursors within the MOF structure by anchoring ALD precursor molecules.

2.3. Gas-phase techniques for deposition of MOFs films

Out of several deposition methods to deposit MOFs films, the liquid phase version has been the commonly used process [69]. The simplest process was to immerse the substrate into a mother solution containing the essential reactants and grow MOFs films under either the typical solvothermal reactions or microwave-induced thermal reactions [70,71]. In order to obtain uniform films and anchor them rigidly to the target substrates, these processes generally involved certain pre-treatments such as deposition of monolayers on the surface on the target substrate surfaces to generate the assisting functional sites [72]. Horcajada et al. demonstrated a colloidal method to deposit MOF MIL-89(Fe) films by dip-coating a gel containing the particular MOF reactants [73]. In another example [74], polymer gel containing metal reactant was firstly coated the on the target substrate, and then the gel as a reaction medium reacted with carboxylic acid solution to form MOF film. In these experiments, liquid-phase deposition methods commonly led to defective MOF films and their adhesion to substrate were not strong

enough. To improve, layer-by-layer liquid-phase epitaxy (LPE) was introduced [75] by Oshekhah et al., and a self-assembled monolayer (SAM) was firstly created on the substrate surface. In their experiments, the reactant solutions were applied on the top in a stepwise manner, and any unreacted reactants in each step was washed off with solvents from the surface. The results showed that the quality of the resulting MOF films was very much dependent on the quality of the SAM layer on the target substrate [76]. Apparently, the liquid-phase reactions with several unpredictive factors could not guarantee the reproducibility of any ideal MOFs films on the target substrates.

Table 1. Comparison between liquid-phase and gas-phase approaches in depositing MOF thin films.

Key features	Liquid-phase Approaches	Gas-phase Approaches	Ref.
Working principle	Spatiotemporal control of the reagents to deposit uniform MOF films under wet chemistry	Spatiotemporal control of the reagents under gas-phase self-limiting growth protocol	[50,57]
Expected properties	Electric conductivity, high break-down voltage, selective molecular sensing, and tuneable dielectric properties.		[51,58]
Surface preparation	Substrates with reactive surfaces are necessary	Substrates with reactive surfaces are necessary	[52,69]
Solvents	Require solvents during the synthesis. Surface-tension phenomena or possible corrosion of the device need to be considered	Require no solvents during the synthesis, and avoid surface-tension phenomena or possible corrosion of the device	[67,70]
Temperatures	Selected MOF thin films can be produced at mild temperatures	Precursors need to be heated to improve the reaction kinetics, which pose challenges for thermally sensitive organic compounds	[68,75]
Depositing area	Usually, very small area can be effectively covered with MOF thin films	Larger area can be effectively covered with MOF thin films	[58,77]
Thickness	Faster diffusion of organic ligands allowing the growth of thick MOF films	Slower diffusion of organic ligands, more effective for thin MOF films	[59,74]
Defect engineering	Can be achieved via in-flow MOF lithography method	Can be achieved via precursor control	[55,56, 58]
Scalability	Have constraints to scale-up cost-effectively	Can be scaled-up with lower cost	[58,79]
Applications	Catalysis, water membrane, organic field effect transistor, selective molecular enrichment, and sensing	Digital and information technologies, dielectrics, barrier layers, capacitors, microelectronics industries.	[50,77]

In contrast (Table 1), as a vapor-phase method for thin film deposition, ALD can deposit thin metal oxide film as precursors for the further growth of MOFs films, and more importantly its self-limiting growth protocol assured the good quality control over MOF films including thickness, composition, conformality, and uniformity [78]. After that, the chemical vapor

reaction (CVR) method can be applied to convert the ALD-deposited precursor films into MOFs crystalline through the vapor-solid reaction mechanism [79]. For instance, a previously ALD ZnO-deposited substrate was suspended in a reactor at 100 °C with vaporized 2-methylimidazole vessel for 30 min, and the ALD-ZnO thin films were successfully converted to MOF ZIF-8 crystalline. Technically, different MOF thin films could also be prepared in this way by ALD depositing different metal oxide layers and then selecting the matching organic ligands. This method has been proved feasible for deposition of MOFs layer on substrates with high-aspect-ratio features such as polydimethylsiloxane (PDMS) pillar [80]. These gas-phased approaches with combined ALD and CVR exhibited some obvious merits over the pure liquid-phase reactions. Piri-Moghadam et al. [81] examined its suitability to coat MOF films for solid-phase microextraction (SPME) Arrow system, but several liquid-phase steps were still involved such as sol-gel dipping. All-gas phase synthesis of SPME Arrow was first documented by Lan et al. [82] who prepared MOFs coatings by using new CVR and ALD-conversion methods, as shown in Figure 7. Fe-BDC coatings in Figure 7 (a,c) were obtained by suspending the ALD-deposited Fe_2O_3 films in vaporized organic ligand of terephthalic acid (H_2BDC), and the UiO-66 MOF coatings in Figure 7 (b,d) were derived by exposing ALD-deposited Zr-BDC film to vaporized acetic acid. In their practices, some difficulties were encountered in the course of coating preparation, which had posed as a technical barrier to be addressed in its further exploitation.

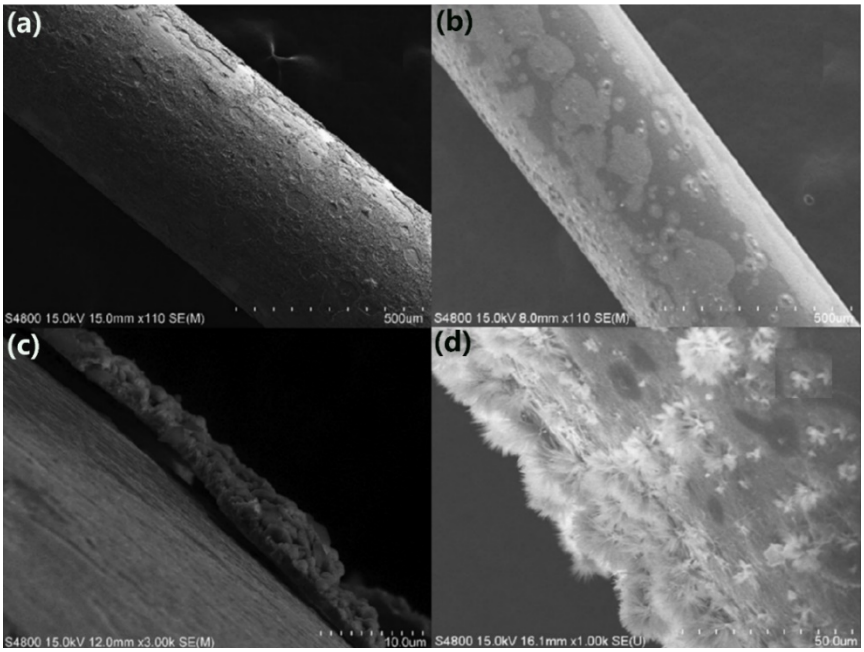

Figure 7. (a-c) SEM images of Fe-BDC, and (b-d) SEM images of SPME Arrows coated with UiO-66(Zr). Reprinted with permission [82]. Copyright © 2018 Elsevier B.V.

2.4. ALD scaling-up solutions

The commercialization potentials of ALD-MOF film processes rely on the current technological readiness and cost levels of the available ALD techniques. Although ALD is a highly effective technique for films coating, there is no set cost for running an ALD-MOF film cycle, and the economic viability of such a process will depend on the design and practical efficiency of the used ALD facilities. In despite of many outlined advantages, the low deposition rate poses as one of the critical disadvantages of this technique and limits its scaling-up to large surfaces or ultra-thick films with high production rates required. Usually, the classic deposition rate of a is at 0.1 nm/cycle, depending on the different ALD settings, 1 h time will only be able to produce Al_2O_3 films with thickness between 100 nm and 300 nm. Although ALD currently is mainly used to coat substrates for high-tech electronics, where ultra-thick film layers are not always required, the scaling-up possibilities will still be reserved as an important factor in actual practices. Besides, many substrates carrying with fragility or purity issues cannot be processed in the normal ALD process, and more advanced ALD processing conditions need to be developed to mitigate these limitations.

2.4.1. Development of advanced ALD process conditions

There are many topics regarding of the development of advanced ALD process conditions. As an important enabler, the availability of precursors will be critical for large-scale ALD process [83]. The common ALD used precursors are volatile, and their controlled decompositions in the set temperature fall into the criteria for the gas-phase reactions. However, their sensitivities to air environment and the resulting decompositions are disfavored by some of the biological applications. As another important enabler, substrate materials for thin-film applications are normally costly particularly those used for microelectronics. Therefore, the continuous development of suitable precursors and cost-effective substrate materials for MOFs device integration will be two parallel tasks. With these in mind, there are necessity to optimize the ALD reaction conditions with focus to: (i) facilitate the optimum coverage of precursor molecules on target MOFs, (ii) introduce active surface sites on MOF particles through the pre-coating of seed-layers, and (iii) create functional groups on MOFs particles by defect engineering.

2.4.2. Design of advanced SALD reactors

Among the efforts focused on the design of more advanced ALD reactor to enable the scaling-up operations, spatial atomic layer deposition (SALD) appeared as a new deposition technology. Despite that SALD had been patented as early as in 1983, the relevant research work was firstly reported in 2008 [84]. Quite a number of patents were filed at the later stage around the further advancements of SALD such as atmospheric pressure ALD (AP-SALD), which was featured

with high suitability and potentials for industrial-scale practices. For example, a close-proximity reactor capable of operating in open-air was filed by Levy (Kodak) [85]. From a technical point of view, SALD shared the same principles with ALD process with regard to surface-terminating reactions, and was able to coat superior-quality films even on nano particles with high-aspect-ratio features at temperatures < 400 °C. In contrast, SALD process did not require the complex and expensive vacuum operations, which resulted in 100 times faster deposition rate than traditional ALD and exhibited a greater potential for scaling-up. In practices, this technique has reached higher TRLs with the ongoing efforts from several companies who have been developing SALD facilities for both laboratory-scale and industrial-scale processes. From the engineering point of view, the SALD approach has been further versified with many reactors developed to date [86,87]. For example, it had been defined as a continuous ALD after precursors were designed to feed into the SALD reactor in a continuous manner. The comparative analysis between ALD and SALD is listed in Table 2.

Table 2. Comparative analysis between ALD and SALD.

	Key features	**Advantages**	**Drawbacks**
ALD	Based on surface-terminating reactions. Precursors were designed to feed in time and separated by purge steps. Up to 0.1 nm/s film growth rate is achievable.	Can be used to coat film thickness of 5–20 nm. Yield high-quality thin films at temperature <400 °C, even on nano particles with high-aspect-ratio features.	Deposition process is typically slow. Require the complex and expensive vacuum operations to be more efficient. Low suitability to operate at atmospheric pressure. Low potential to scale up. Require for suitable substrate and less precursors are available. Practices remained at low TRLs.
SALD	Based on surface-terminating reactions. Precursors were designed to feed continuously but separated in space by different slots. Up to 10 nm/s film growth rate is achievable.	Yield high-quality thin films at temperature <400 °C, even on nano particles with high-aspect-ratio features. Does not require the complex and expensive vacuum operations. High throughput and much faster deposition. High suitability to operate at atmospheric pressure. Greater potential to scale up. Practices have reached higher TRLs.	Require precursors of high volatility. The number of available precursors is limited. Often sensitive to oxygen or water when processing in air.

As shown in Figure 8, the dosing of precursors from the traditional ALD design was commonly separating in time with purging steps, while the spatial ALD (SALD) was designed to receive constant dosing of precursors but moving between different precursor regions (Figure 8a). More importantly, the typical time-consuming purge steps in ALD processes were no longer required in a SALD process, which led to a 100 times faster deposition rate than ALD. Furthermore,

SALD had the convenience to be operated at an ambient atmosphere, and scaling-up SALD was much easier and cheaper compared to the conventional ALD. All those merits built-up the foundation for SALD to be widely used as a reliable coating technique in industrial practices. As a follow-up, a circular reactor was developed for flexible substrates by the Lappeenranta University of Technology [88]. In their design, the flexible substrate by design could be attached to a cylindrical drum, which would rotate inside a reaction chamber to dose and purge different precursors. Such a film coating process was similar to any other ALD, and the film would grow on the basis of surface-limiting reactions per cycle, i.e. for the typical deposition process of Al_2O_3 film, a deposition rate of 0.1 nm per cycle could be achieved at 100 °C by using the ideal trimethylaluminum (TMA)/water system. A modular rotating cylindrical reactor developed by the University of Colorado (Figure 8b) was configured with two concentric cylinders: (i) the various spatially separated slots attached to the outside of the fixed outer cylinder allowed to accommodate different modules. These modules were switchable around different slots to fulfil the pumping, dosing, and purging operations. (ii) the rotatable inner cylinder would rotate to allow the flexible target substrate to pass at the set speed under the shots in the fixed outer cylinder. With inner cylinder at a rotation speed of 175 rounds per minutes (RPM), the same TMA/water deposition process could grow Al_2O_3 films at a rate of 0.2 nm/s at 100 °C, and higher deposition rates were also achievable by increasing the flow rate of precursors. Figure 8c (left) showed two designs based on AP-SALD [84], wherein the coating heads were designed to dose different precursors through separated channels. The adjoining channels were designed to supply inert gas flows such as N_2 and also was responsible for the separation of different precursors. As noticed, such design did not feature a deposition chamber, and the film growth was achieved simply by repeating ALD cycles between the coating head and the motion of substrate. As a result, this reactor could be potentially operated in the open air. It's worthy to mention that in the first design the coating head was placed on the top of the moving substrate, while it was changed to the bottom in the second design with outlets facing upward to the moving substrate. Later, similar SALD setup (Figure 8c, right) was developed by the Laboratory of Materials and Physical Engineering (LMGP) in France [89]. By now, SALD approach has readily been scalable for multiple applications by compatible with other processing methods i.e. roll-to-roll ALD processing platform.

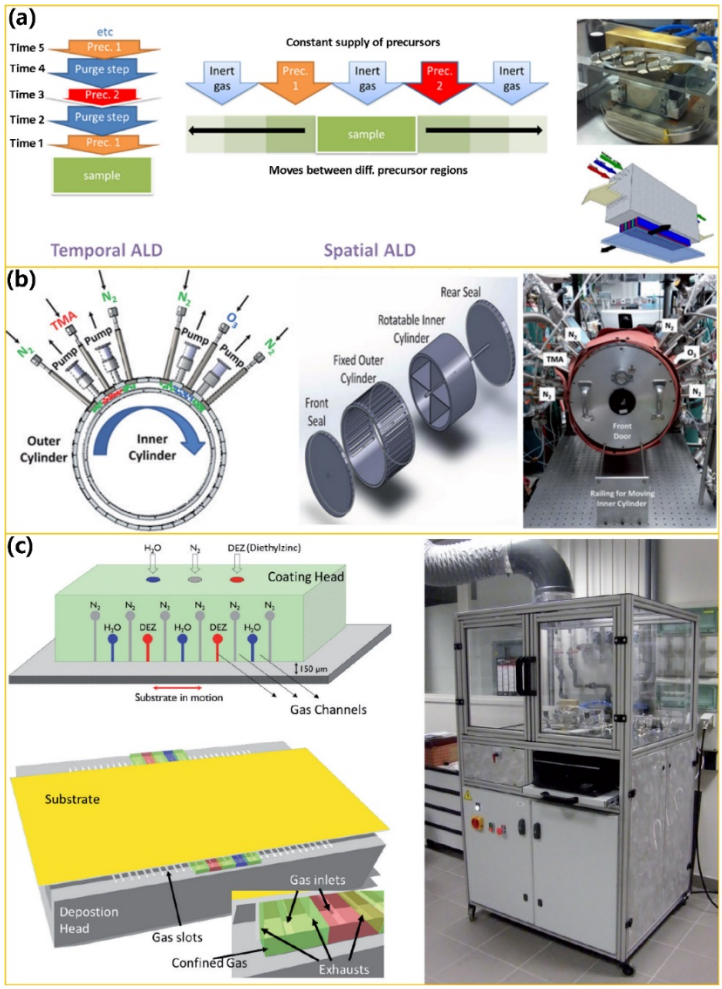

Figure 8. (a) The difference between SALD and ALD. Reprinted with permission [24]. Copyright © 2017, Académie des sciences. Published by Elsevier Masson SAS. (b) University of Colorado configured SALD. Reprinted with permission [88]. Copyright © 2015 American Vacuum Society. (c) Kodak-developed close-proximity SALD (left), and LMGP-developed SALD system (right). Reprinted with permission [89]. Copyright © 2019 Intech Open.

2.5. Characterization techniques for ALD MOF films

To assure a highly precise ALD-MOF film work, the quality monitor and control on the ALD-deposited thin MOF films lie on the availability of characterization techniques. In literature, the growth dynamics of the ALD-MOF film deposition was obtained by the in-situ quartz crystal microbalance (QCM), and mechanical properties of ALD-deposited films were derived from Nanoindentation. Besides, the textural-relevant properties including film thickness, refractive index, surface morphology, BET surface area, film density, pore size distribution, roughness, as well as the chemical composition and coverage analysis of the MOF films are typical parameters of interests to researchers.

2.5.1. Textural properties

In the work of Langereis et al. [90], the ALD-deposited MOF film thickness as well as refractive index were characterized with an ellipsometry and a programmed spectrophotometer (Hitachi U2000, λ= 370~1100 nm). Usually, the morphologies of the ALD-deposited MOF films were observed by scanning electron microscopy (SEM) and atomic force microscopy (AFM). While the film geometries, variation of film thicknesses, microstructure of thin films, possible interfaces, substrate dislocations, and grain sizes were analysed by transmission electron microscopy (TEM). In some cases, TEM was used to analysis oxide thin films and their heterostructures. The Brunauer-Emmett-Teller (BET) surface area of ALD-deposited sample could be obtained from a BET analyser, and Micromeritics Accelerated Surface Area and Porosimetry (ASAP) could provide a comprehensive analysis on BET surface area and data set for pore size distribution. During the adsorption/desorption experiments, N_2 gas was commonly used for to obtain the isotherms. Sometimes, Ar or Kr gas was used to allow more sensitive measurement in case the BET surface area of the sample was very low. Besides, some other characteristics of the ALD-MOF film sample including film thickness, density or surface roughness could be studied in details by X-ray reflectivity (XRR).

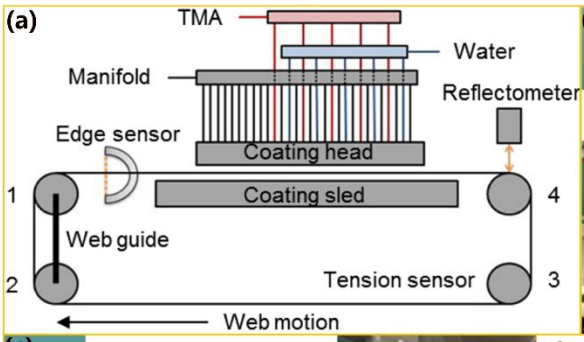

(d)

Sample	In-situ reflectometry moving web (nm)*	In-situ reflectometry stationary web (nm)*	Ex-situ ellipsometry (nm)	SEM (nm)
I	52	51		~50–53
II	105	105	101 ± 7	
III	184		188 ± 3	

* The standard error of the reflectometer was ± 2 nm

Figure 9. An AP-SALD reactor configured with in-situ film thickness monitoring system: (a) Schematic of the AP-ALD web-coating reactor, (b) Photo of the used coating head. (c) Reflectometer (FilMetrics F20-UV) measurement setup. (d) Comparison of several measurement techniques on Al_2O_3 film thickness. Reprinted with permission [91]. Copyright © 2014 American Vacuum Society.

The real-time monitoring of film thickness by using a spectral reflectometry was demonstrated by Yersak et al. [91] in-line an AP-SALD (Figure 9). As shown in Figure 9a, Al_2O_3 film was

deposited on polyethylene naphthalate (PEN) substrates with TMA and H_2O as precursors at 100 ºC. The derived results from the in-situ measurement were assisted to optimize process parameters including coating head configurations, gap height between coating head and coating sled, web moving speed, flow rate of precursor, coating temperature, and substrate materials. In a typical process, the polymer web was ALD coated with Al_2O_3 film while it was continuously passing through the outlets in the coating head, and the ALD coating head in Figure 9b were configured with 5 ALD TMA/H_2O cycles and N_2 as the purge gas. The configured reflectometer was capable of measuring ALD film thicknesses in the range of 2–40 nm. As illustrated in Figure 9c, the fiber optic cable transmitted the light beam with a wavelength of 200–1100 nm and focused it onto the substrate at a designed angle. The in-line spectrometer received the reflected light back from the substrate and measured its intensity at 512 different wavelengths. Then, the built-in modelling software calculated out the film thicknesses. The vendor stated error of this testing system was 62 nm for film thickness <500 nm and 0.4% for films >500 nm. To validate the reliability of the in-line reflectometer, a standard Si wafer (SiO_2 = 724.7 nm) was used as reference in experiments. The Table in Figure 9d listed the comparative results of a film thickness obtained respectively from the real-time reflectometry on a moving web, ex-situ ellipsometry, real-time reflectometry on a stationary web, and cross-sectional SEM tests. Given the standard error of the reflectometer of ±2 nm, these four techniques agreed well with each other, which validated the employment of reflectometer for real-time monitoring of ALD film thickness.

2.5.2. Chemical composition and Coverage analysis

In literature, the chemical compositions of ALD-deposited films were usually determined by different technique combinations. Typically, the crystallinity and any impurities in the MOF films was identified by powder X-ray diffraction (PXRD). In contrast, the surface crystallinity of an ALD film was usually determined by the grazing incidence wide angle X-ray scattering (GIWAXS). The presence of any functional groups and molecular components in the ALD MOF films were commonly identified by Fourier-transform infrared (FTIR), and Roman spectroscopy would provide the chemical and structural information. For some special interests, the level of hydration after the water cycle in the ALD process could be revealed by diffuse reflectance infrared Fourier transform (DRIFT) spectra, and variable temperature DRIFT measurements could identity the hydroxy functionalities. Except for the thermal stability, thermogravimetric analyses (TGA) could also probe the fraction of volatile components in the sample by monitoring the weight change with increasing heat temperature. In some cases, the elemental composition of MOF films was determined by X-ray fluorescence (XRF) as one of the non-destructive analytical techniques. The content and purity of a film sample could also

be detected by nuclear magnetic resonance (NMR). To quantify the elemental composition of a film sample, energy dispersive X-ray spectroscopy (EDS) was commonly used, while inductively coupled plasma-optical emission spectroscopy (ICP-OES) could handle the analysis at trace-level. Selected-area electron diffraction (SAED) was usually coupled inside a TEM test to obtain diffraction patterns that scattered by the sample lattice. Gas chromatography and mass spectrometry (GC-MS) together were often used to identify and quantify different organic components in an ALD film. To readily observe interface between ALD deposited-film and MOF surface, the scanning TEM (STEM) with a z-contrast image or cross-sectional high-resolution TEM (HRTEM) were recommended.

Sometimes, the ALD cyclic numbers with full film coverage could be determined by X-ray photo-electron spectroscopy (XPS), for instance, by acquiring XPS spectra from the ALD-deposited Al_2O_3/Si sample after each ALD cycle, the amount of deposited Al_2O_3 film and its thickness information could be quantified over the length of the ALD process. Thermo Scientific™ Nexsa XPS system added the capability of other technique analysis such as ion scattering spectroscopy (ISS). Compared to XPS, ISS extracted spectral information only from the top monolayer of the ALD film sample. In other words, ISS was able to analyse the energy of the scattered ions to reveal the elements presented in the top monolayer of the sample. Bear this in mind, any picking-up of the substrate Si signal would imply the incomplete coverage of the Al_2O_3 film deposition. By following this clue, the intensity of the substrate Si signal would be reducing with the increasing ALD cycles, and the exact ALD cyclic number of reaching the full Al_2O_3 film coverage on Si substrate could be obtained when the substrate Si peak started disappearing completely from the spectra.

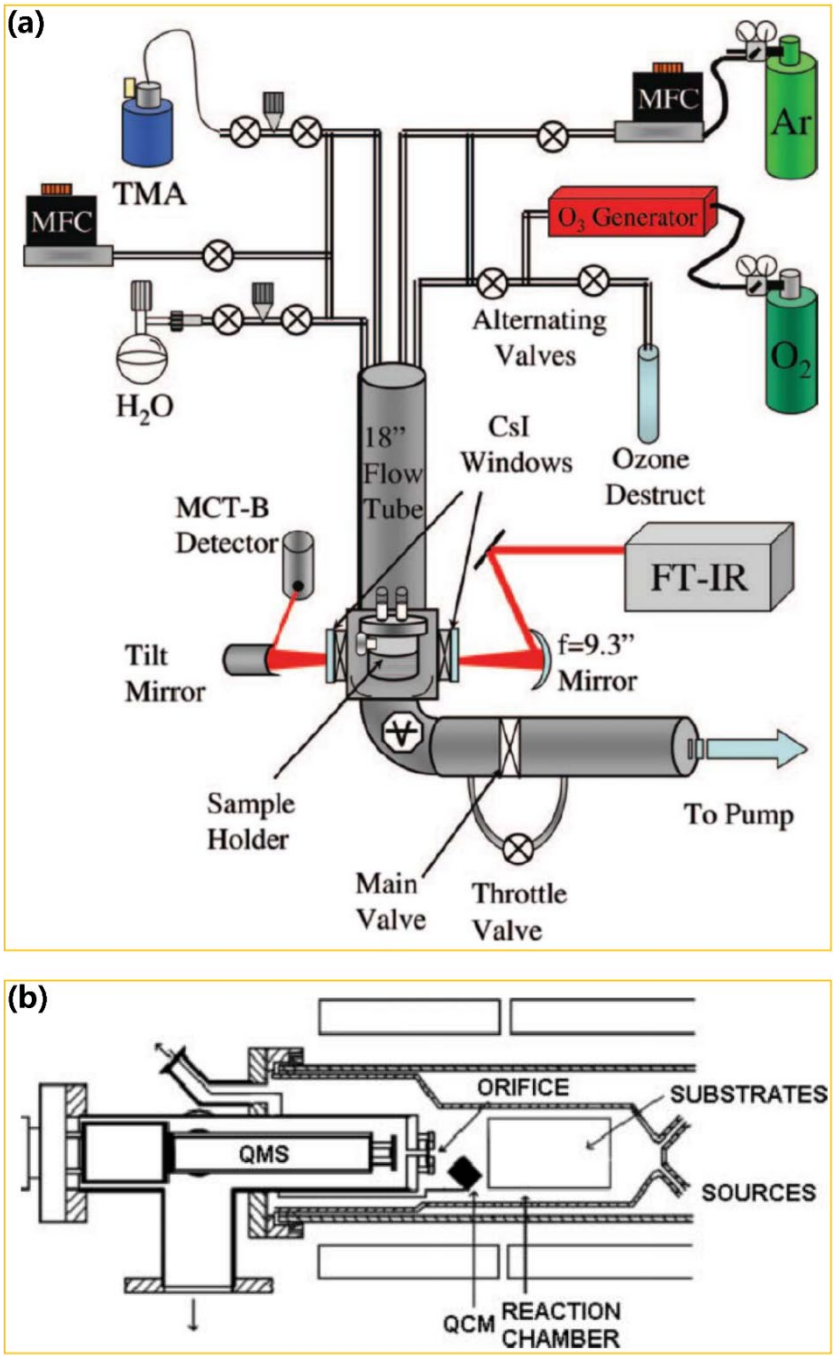

Figure 10. (a) An example of ALD-FTIR spectroscopy system. Reprinted with permission [92]. Copyright © 2008 American Chemical Society; (b) An example of ALD-QMS-QCM system. Reprinted with permission [93]. Copyright © 2009: John Wiley and Sons.

As shown in Figure 10, some studies have employed real-time characterization systems to control the quality of the ALD-deposited films. Figure 10a showed the integration of FTIR as an in-situ characterization system in an ALD process, and the FTIR spectroscopy was taken real-time to characterize the gaseous species generated in the sample holder. Similarly, since quadrupole mass spectrometer (QMS) could in-situ analysis the gas composition inside the process chamber during the ALD deposition of thin films, the in-situ ALD-QMS-QCM in

Figure 10b were applied to provide the real-time monitoring of the ALD-MOF film processes by exploring the nucleation and growth of the films. Besides, Knapas et al. [94] investigated the electronic and geometric structure of ALD films by in-situ studying the specific structures including X-ray absorption near edge structure (XANES) and X-ray absorption fine structure (EXAFS) that observed in the X-ray absorption spectroscopy (XAS).

2.6. Toxicity evaluation on MOFs device integration

With time going, MOFs has been extensively researching worldwide as a new family of nanomaterials, and they have become a source of nanoparticles exposure to humans. Such human exposure can occur at any stage during the life cycle in the course of lab-scale MOFs synthesis, up-scaled manufacture, device integration, usage, and disposal. The introduction of MOFs nanoparticles into the work environment and consumer products necessitated safety evaluations as well as a clear understanding of any potential impacts on animal and human health. As exposure of MOFs nanoparticles mainly occurred through respiratory route, and they had the potential to pass through biological membranes to affect and compromise the physiology of any cell in animal or human bodies, such potential of MOFs ingredients to enter biological systems poses a matter of great concern to the general public [95]. However, the currently available data from the published information around the toxicological effects and risk assessment of MOFs nanoparticles to safety, health and environment (SHE) is very limited. Given the possibility that customer can be exposed to any MOF-integrated products such as surface coatings, therefore, relevant studies on the toxic effects of MOFs device integration shall be conducted to provide an understanding of possible toxicity mechanisms. Any concluded suggestions from the toxicity evaluations will be helpful to improve the biological safety and guide the relevant activities for MOFs device integrations. The evaluation modules can be referred to the work conducted on the graphene-family nanomaterials [96,97].

3. Practices for ALD-MOFs devices integration

The outperformed characteristics of MOFs over the traditional materials i.e. zeolite and carbon have provided the potentials for novel applications or at least performance improvement [98–103]. Up to now, most of the studies on MOFs in applications are mainly in their powder forms i.e. their applications in materials-based gas storage options or adsorption of heavy metal ions in water treatment. Any further devices integrations in electronic, magnetic, and optical fields require thin MOF films or membranes with incorporated chemical functionalities. ALD is believed to be an enabling technique for the further advancements of MOFs chemistry towards the targeted applications [104].

3.1. ALD post-synthetic functionalization of MOFs

The post-synthetic functionalization of MOFs has been recognized as an effective approach of tailoring the MOFs properties towards the envisioned applications of interests such as MOFs in catalysis by serving as catalysts supports, nanoconfinement geometries, or catalytic species themselves [105]. To precisely tailor MOFs' properties for target applications, ALD as one of the post-synthetic functionalization approaches in this aspect offered a rich platform to advance this field by materials design and surface engineering. AIM is one important emerging advance to leverage and enrich the existing palettes between ALD and MOF chemistries.

3.1.1. ALD functionalization of MOF linkers

Differing from the traditional liquid-based methods to modify the MOF linkers [106–109], Klepper et al. [110] have further expanded this field by ALD depositing thin films using TMA and carboxylic acid system. Their study tested 7 acids including sebacic acid, oxalic acid, succinic acid, malonic acid, glutaric acid, suberic acid, and pimelic acid, and all the ALD film growth rates showed dependence on the processing temperature. Out of 7 systems studied, the TMA/pimelic acid system displayed the highest film growth rate of 4.3 nm per cycle, and a correlation between he ALD window width and the carbon chain length were observed. The complex nature of the obtained ALD films with bridging complexes was proved by FTIR tests, however, no obvious diffraction signals were observed in the XRD measurements, implying the amorphous phases for all the as-prepared films. The water stability testes showed that the deposited films from two systems of TMA/oxalic acid and TMA/malonic acid were unstable, and all others were stable in water.

3.1.2. ALD functionalization of MOF nodes

Often, the unsaturated metal ions in MOF structure enabled the functional behavior of MOFs materials, and the enhanced chemical competency were observed from metalated MOFs in different scenarios [111]. In literature, techniques that commonly used for functionalization of MOF nodes covered solvent-assisted ligand incorporation (SALI) [112], solvothermal deposition in MOFs (SIM) [113,114], AIM, and metal-ions exchange (ME) [115,116]. The main route for SALI was to functionalize MOF nodes with different organic groups, while SIM, AIM, and ME tended to functionalize MOF nodes with different metals. Wherein, ALD was used to attach metals and metal clusters by design to the MOF nodes, so as that the resulting MOF hybrids exhibited some unique catalytic properties [117–119]. The relevant work started with the ALD deposition of Al_2O_3 thin films on Ag nanoparticles (NPs), and subsequently the deposited Al_2O_3 film was converted to Al-MOF [120, 121]. For instance, Guntern et al. [122] deposited Al_2O_3 thin films by using ALD on Ag NPs and then solvothermal converted the films to Al-MOF via colloidal chemistry to fabricate Ag@Al-PMOF hybrids (Figures 11).

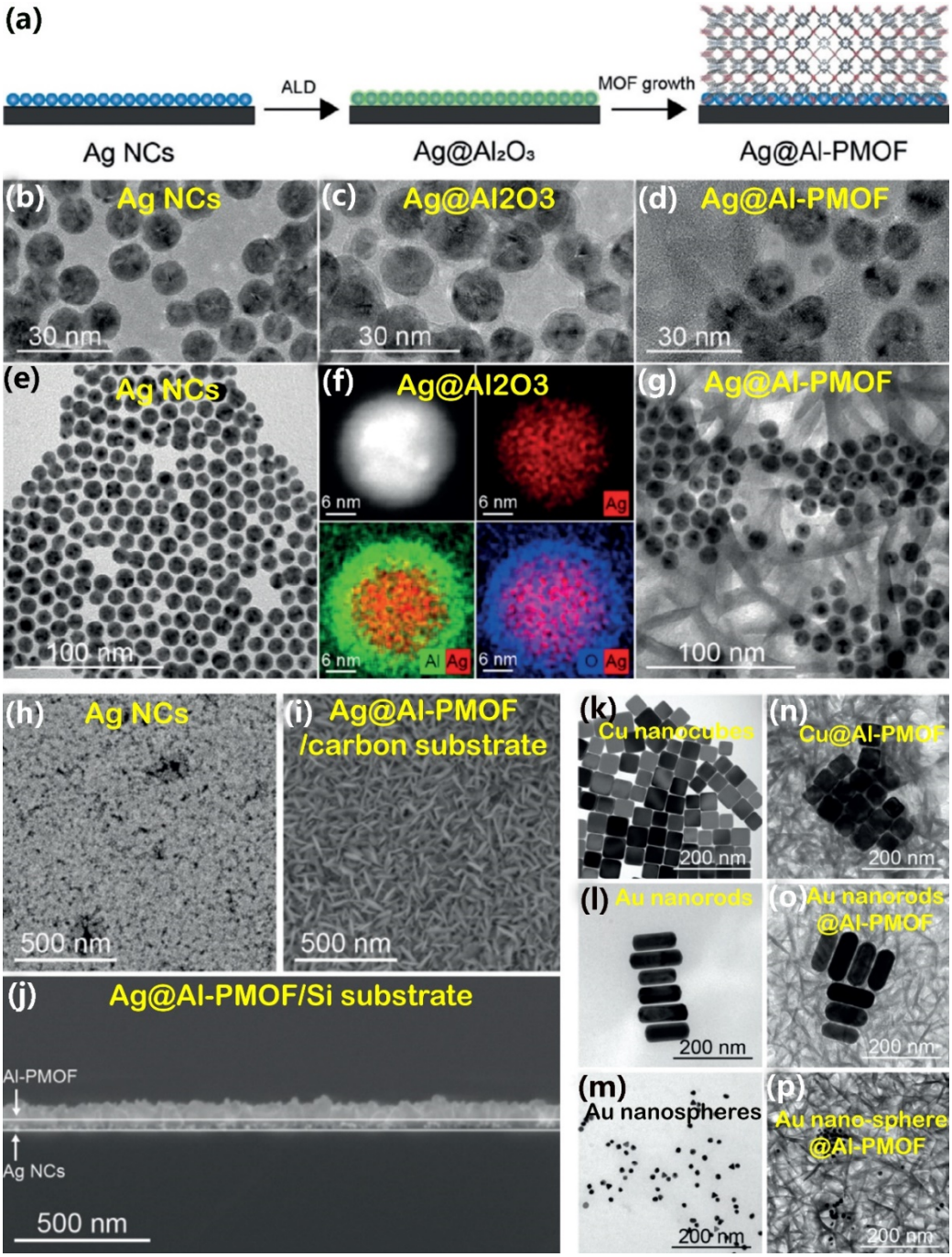

Figure 11. (a) Synthesis route of Ag@Al-PMOF hybrid. (b-p) The stepwise electron microscopy images. Reprinted with permission [122]. Copyright © 2019, Wiley-VCH Verlag GmbH &Co. KGaA, Weinheim.

In their study, spherical Ag nanoclusters (NCs) with multiple-twinned structure were firstly drop-casted on several substrates including silicon, copper TEM grid and glassy carbon. Then, Al_2O_3 shell was coated on the NCs by ALD to form Ag@Al_2O_3 core@shell structure. Eventually, Ag@Al-PMOF hybrid was obtained by converting Al_2O_3 shell into Al-PMOF in a microwave reactor through a reaction with 5,10,15,20-tetrakis(4-carboxyphenyl)porphyrin (TCPP) linker in a dimethylformamide (DMF)/H_2O solvent mixture. Figure 11a displayed the

reaction route for the Ag@Al-PMOF hybrids, and Figures 11b–g showed the stepwise electron microscopy images. As observed, Ag NCs were completely wrapped by a 3 nm thick Al_2O_3 shell after 45 ALD cycles with an interface visible, and most of their shapes were retained during the process of Al_2O_3 deposition. After the conversion, a uniform 50–80 nm layer consisting of plate-like MOF crystallites were revealed in Figure 11h–j. Finally, the generality of this synthesis approach was applied by authors onto Cu NCs, Au nanorods and Au nanospheres to synthesize hybrids of Cu@Al-PMOF, Au nanorods@Al-PMOF, and Au nanospheres@Al-PMOF. Their structures could be seen in Figures 11k–p, where different NCs were wrapped around by uniform layers of Al-PMOF crystallites.

The reactions between ALD precursors of $InMe_3$ and $AlMe_3$ with the nodes within MOF NU-1000(Zr) were monitored by Kim et al. [123]. It's noted that stable structures were formed with MOF crystallinity and textural properties nearly intact after the reactions. The experimental analysis by X-ray pair distribution function (PDF) well predicted the final structure. The different metal loadings were achievable by the dehydration of MOF nodes at elevated temperatures to adjust the number ratios between OH and $-OH_2$. In a single ALD cycle of $InMe_3$ reacting with MOF NU-1000(Zr) nodes, it was possible to reproduce the modulation of the stoichiometry by partially dehydrating the nodes with controlled temperatures. Apparently, this concept would allow to design ALD process with multiple metal precursors. Later, the same group [124] deposited catalytic Pt clusters onto the NU-1000(Zr) MOF nodes by following the similar procedure, and the analysis revealed the presence of either atom clusters or single atoms under different synthesis conditions. The resultant hybrid catalyst was tested with high catalytic performance for the hydrogenation of ethylene. These results demonstrated AIM would be a suitable approach to probe the loading mechanism of target metals or metal clusters on MOFs-type substrates with large BET surface areas. Yang and co-workers [125] also functionalized the MOF node by ALD incorporated hydroxylated Al^{3+} ions in MOFs. Another interesting work was done by Platero-Prats et al. [126] who used ALD deposited Ni_4-based clusters to bridge Zr_6-nodes within MOF NU-1000(Zr) structures and obtained heterobimetallic nanowires along the c-direction, as shown in Figure 12. Their comprehensive analyses indicated that the NiO_xH_y clusters were selectively attached onto Zr_6-nodes within the small pores of NU-1000(Zr) MOF structure, and heterobimetallic metal-oxo nanowires could be formed along the c-direction with those connections. Such understanding on the structures of ALD-deposited metal oxo clusters and how they selected active sites within a MOF structure was critical to engineer the material properties.

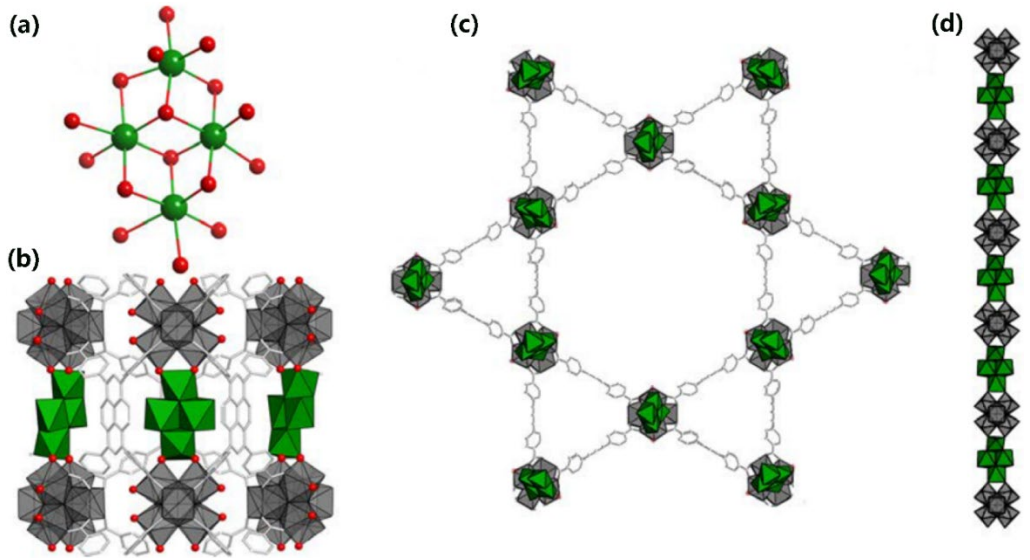

Figure 12. (a) Atomic structure of ALD-deposited $Ni_4O_xH_y$ cluster derived from DFT calculations in the MOF NU-1000(Zr) structure. (b) Parallel view of the distribution of Ni_4-based clusters, (c) Perpendicular view to the c-axis, and (d) Heterobimetallic nanowires formed [O: red; C: light grey; Zr: grey; Ni: green]. Reprinted with permission [126]. Copyright © 2017 American Chemical Society.

Although theoretical investigations on functionalization of MOFs with metal-inorganometallic nodes remained as challenge due to the complex nature of species containing transition metals, they were of particular aid in rationalizing observations on geometric and electronic configurations of hybrid catalysts to predict their catalytic selectivity or activities. More importantly, theoretical studies were able to provide valuable information to guide experimental work designs and validate the experimental results, or even suggest experiments that not yet conceived. Therefore, functionalization of MOF nodes could be the way to engineer catalyst by design. For example, quantum mechanical modelling was used by Bernales et al. [127] to validate experimental results and maximize the potential of MOFs with outperformed catalytic activity. In-situ PDF and DFT analyses were employed by Platero-Prats et al. [128] to probe the possible structural transitions of Zr_6O_8 within UiO-66(Zr) and Hf_6O_8-nodes within NU-1000(Hf) MOF structures. Although the structures of those two nodes were found to transit, the symmetries of UiO-66(Zr) and NU-1000(Hf) MOF frameworks did not change at temperatures that were suitable for most of the MOF applications. Moreover, the distortion of nodes was observed to occur in a MOF framework at much lower temperatures than those in ZrO_2 with bulk structures, and the nano-porous characteristics of MOF materials was account for such difference.

3.1.3. ALD metalating MOF materials

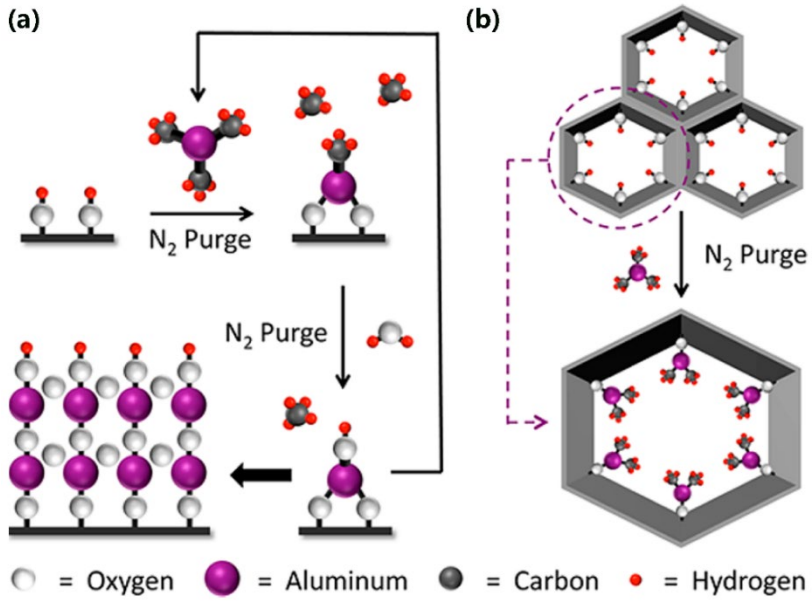

4. 5.

Figure 13. (a) ALD thin film deposition on a target substrae, and (b) Illustration of ALD metallating a MOF. Reprinted with permission [63]. Copyright © 2013 American Chemical Society.

Relying on the repetition of ALD precursor and water dosing cycles, AIM offered a gas-phase strategy to metallate a target MOF, as illustrated in Figure 13. In the AIM strategy of Bhattacharya et al. [129], the MOF secondary building units (SBUs) were synthesized by incorporating Ba^{2+} ions into the compound of polyoxo-13-palladate(II) nanocubes $[Pd_{13}O_8(AsO_4)_8H_6]^{8-}$, and the metalated polyoxopalladate (POP)-based MOF framework was obtained through the linkages of those SBUs. The resultant MOF structure was proved to be stable with interesting sorption and catalytic properties. He and co-workers [130] screened 3000 types of MOFs by using an approach called transfer learning strategy, which consisted of statistical multivoltine, machine learning techniques, and ab initio calculations. Out of those screened MOF samples, six MOF structures including $Mn_2[Re_6S_8(CN)_6]_4$, $Mn_2[Re_6Se_8(CN)_6]_4$, $Mn_2[Re_6Te_8(CN)_6]_4$, $Mn[Re_3Te_4(CN)_3]$, $Hg[SCN]_4Co[NCS]_4$, and CdC_4 were identified to be metallic at the level of semi-local DFT band theory. Some patents also described the similar content focused on the approach to metallate MOFs [131]. Hupp group [132–136] has done a lot of work in this area, for example, they reported the fabrication of Cu nanoparticles@MOF, wherein the diameters of metallic Cu nanoparticles were very dependent on the pore sizes of the working MOF. In a typical process, Cu(dimethylamino-2-propoxide)$_2$ molecules permeated the MOF NU-1000 (Zr) structure and reacted with aquo and hydroxo ligands within Zr_6-MOF nodes. Then, the residual dimethylamino-2-propoxide ligands was removed by dosing with steam, and simultaneously the vacant sites were replaced by both aquo and hydroxo ligands. By now, the Zr_6-nodes within MOF NU-1000 (Zr) structure were found to alternate with tetra-

copper(II)oxy clusters along the c-axis direction. The Cu^{2+} ions could be reduced to Cu atoms by H_2 gas under a pre-determined temperature, and Cu particles formed within the MOF pores through the movement and agglomeration of the neutral Cu atoms. Due to the effect of confinement, the sizes of Cu particles would stop growing when they reached the dimensions of the corresponding MOF NU-1000 pores.

3.1.4 ALD combines with molecular layer deposition (MLD)

Similar to an ALD process, MLD also works under the sequential models of dosing reactants, and the surface reactions are self-limiting nature. The only difference lies in that ALD uses metal-organic precursors while MLD uses organic compounds. In other words, if ALD can be called as an advanced CVD method, MLD can be considered as an ALD-derived method [137]. Through MLD process, purely organic and organic-inorganic hybrid films can be obtained with good conformality and thickness control [138]. Although it is technically feasible for MLD to prepare numbers of metalcone materials, in literature, alucone was the most common material that synthesized by using TMA as metal precursor and ethylene glycol (EG) as organic reactant [139,140]. With the combination of ALD and MLD techniques, it became possible to make multi-layered or other structures by design. Both of their self-limiting cyclic processes would contribute together to the film growth with well controllable thickness and conformality. By following this thought, it was also workable to make nano-laminating films, thin-film mixtures, and designed patterns on the target substrates by adding different materials. For example, the post-deposition wet etching processes and heat treatment have been demonstrated by Van de Kerckhove et al. [141] to keep porous oxide backbones by selectively removing the organic part from the ALD/MLD inorganic–organic hybrid material.

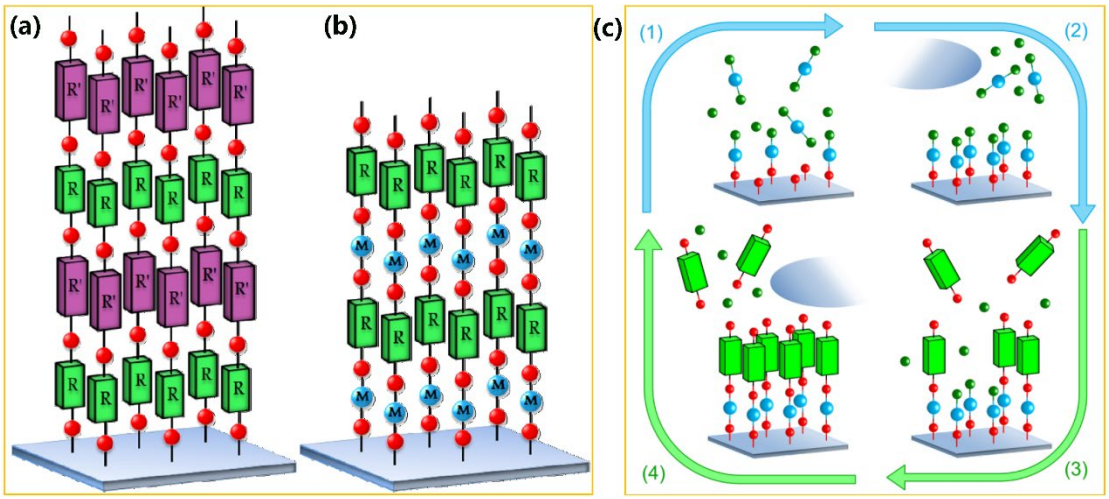

Figure 14. (a) MLD grows purely organic thin films, (b) ALD/MLD grows hybrid inorganic-organic thin films, and (c) Four steps in an ALD/MLD cycle. Reprinted with permission [142]. Copyright © 2014 Sundberg and Karppinen.

Figure 14 illustrated an ALD/MLD process where organic molecules and metal atoms were covalently bonded together. Either interlinked hybrid inorganic–organic polymer chains or alternating monolayers could form hybrid thin-film structures, which would have the complementary properties from two individual materials, or even completely new material properties for the designed purposes (Figure 14 a–b). As shown in Figure 14 c, although the combined ALD/MLD process might employ different inorganic-organic precursors, the precursor dosing and intermediate purging steps remained as the same. Since both ALD and MLD were subject to surface reactions in the sequential and self-limiting manner, good quality control could be achieved on the grown films. Therefore, their combinations could be a great asset for MOFs technology and device integration.

3.2. ALD confinement of nanocatalysts into MOFs

As known, space-confined catalysis has been adopted as a viable strategy to tailor the catalytic properties of various catalysts. To achieve such goal, finding a confined space to be the second coordination sphere around the selected catalyst was crucial. Typically, the confinement of catalysts into MOF structures can be achieved by traditional liquid-phase methods. On one hand, the excess metals, unreacted reagents or undesired solvents much be removed from the supporting material after the synthesis. On the other hand, it also showed difficulty in precisely regulating the confined nanostructures and assemble multifunctional sites in the confined nano-spaces. Due to the outstanding advantages, ALD is expected to provide a more controllable method to confine catalysts into MOFs structures.

3.2.1. Metal oxides

For microporous MOFs materials with large aspect ratios and small pore sizes, it remains a challenge to deposit ALD species uniformly into the confined space due to the diffusion limitation of precursor molecules. Gao et al. [143] implied that the ALD precursor molecules preferred to deposit only at chemically reactive sites within a MOF structure. Some research groups have successfully confined nano-catalysts with interests into MOF structures. For instance, Rimoldi et al. [144] confined Al_2O_3 particles into MOF Nu-1000 (Zr) structure by using dimethylaluminum iso-propoxide (DMAI) as an ALD precursor, and the resultant hybrid catalyst outperformed γ-Al_2O_3 with increased selectivity. Peters and co-workers [145] ALD confined mixed-metal NiS_x clusters with active sites into NU-1000(Zr) MOF structure as the low-cost photocatalytic catalyst for H_2 evolution. Klet et al. [146] used AIM/ME combined approach to atomically disperse Zn atoms into the mesoporous MOF Nu-1000(Zr), and subsequent transmetalation allowed the replacement with nano-structural Cu, Co, and Ni. Palmer et al. [147] used ALD to install ZrO_2/C into Nu-1000 (Zr), and the pyrolysis-derived material at 900 °C under N_2 was found to have high electrocatalytic activity for oxygen

evolution. Rimoldi et al. [148] deposited the ReO_x catalytic functions into Nu-1000(Zr) MOF with catalytically active for ethane hydrogenation. Peters et al. [149] incorporated catalytically active Co_9S_8 with the high surface area into Nu-1000 (Zr) MOF by ALD to selectively hydrogenate m-nitrophenol to m-aminophenol. Li et al. [150] deposited Ni^{2+} ions onto the Zr_6-nodes within UiO-66(Zr) MOF structure by an ALD-kind method for ethylene hydrogenation. Two post-synthetic methods of AIM and solution-phase grafting were employed by Ahn et al. [151] to graft Nb_2O_5 sites onto the Zr_6-nodes within MOF NU-1000(Zr). The DED measurements suggested that Nb(V) ions displayed with two different structures within NU-1000(Zr) from the two different methods. MOF-supported catalysts showed higher selectivity and activity for cyclohexene epoxidation with aqueous H_2O_2 than those of Nb-ZrO_2 catalyst.

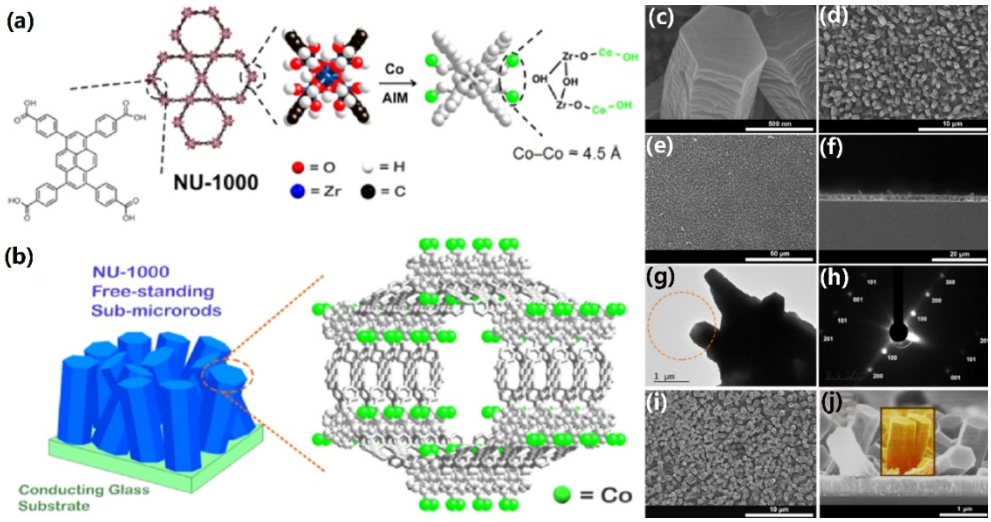

Figure 15. (a) One possible configuration after Co-AIM within MOF NU-1000(Zr), (b) MOF NU-1000(Zr) film with free-standing atomic cobalt, (c−f) SEM images of MOF NU-1000(Zr) film, (g,h) TEM image and SAED pattern of MOF NU-1000(Zr) microrods, (i) SEM image and EDS elemental mapping of AIM Co-NU-1000(Zr) film (Co: green; Zr: red). Reprinted with permission [153]. Copyright © 2015 American Chemical Society.

As commonly recognized, the encapsulation of a nanosized catalyst in a confined space < 1nm provided a strategy to preserve their nano-scale feature, which has been believed to be crucial in conferring their unusual properties. Rimoldi et al. [152] used tetramethoxysilane ($Si(OMe)_4$) as an ALD precursor to confine SiO_x units into MOF NU-1000(Zr) structure. Although the bulk SiO_2 alone was inactive, the obtained Si-AIM NU-1000(Zr) hybrid material exhibited catalytical activity with nanoscale effects from nanosized SiO_x clusters. The author concluded that the unusual electronic properties from the nanoscale SiO_x clusters together with the electron-donating nature from Si-AIM NU-1000(Zr) were responsible for the resulting high catalytic activities. The results also indicated that ALD SiO_2 into a Zr-MOF could be a way to enhance its acidity. Kung et al. [153] chemically grew high-porosity MOF NU-1000(Zr) films

onto glass substrate coated by fluorine-doped tin oxide (FTO) with transparent and conducting nature. Subsequently, Co^{2+} ions were incorporated by AIM to enable electrocatalytic water oxidation. As illustrated in Figure 15 a–e, MOF NU-1000(Zr) films uniformly covered the transparent glass with no bare area observed, which in turn were used as supports to anchor catalytically competent Co ions. With similar anticipation from other electrode coating approaches, the hybrid of FTO-glass coated with MOF NU-1000(Zr) thin films was expected to enrich catalytic sites on surface of the target electrode. Meanwhile, those catalyst sites in a highly porous MOF scaffold were believed to be capable of being reached easily by the chemical reagents in the electrocatalytic processes. Figure 15f–h showed a uniform hexagonal shape of MOF NU-1000(Zr) film deposited on the FTO substrate. Furthermore, Noh et al. [154] successfully employed vapor-phase AIM and condensed-phase SIM approaches to impregnate metal-containing species into MOFs as heterogeneous catalysts.

3.2.2. Single-site anchor

For a better design of outperformed catalysts, the ability to develop the single-site supported catalysts will ensure the detailed mechanistic studies. In that regard, the AIM strategy to anchor single sites to MOFs nodes has been recognized by two review articles [155,156], and several research groups [157,158] have done great work in this aspect. For instance, Li et al. [159] anchored ALD-Ni ions uniformly to the Zr_6-nodes within Nu-1000(Zr) MOF structure, and the resultant Ni-AIM Nu-1000(Zr) MOF was proved efficient for ethylene hydrogenation. The Ni ions that isolated in MOF structure showed long-term stability throughout the hydrogenation catalysis, and the turnover frequency (TOF) for Ni-AIM Nu-1000(Zr) MOF catalyst was 10 times that of ZrO_2-supported nickel metal nanoparticles.

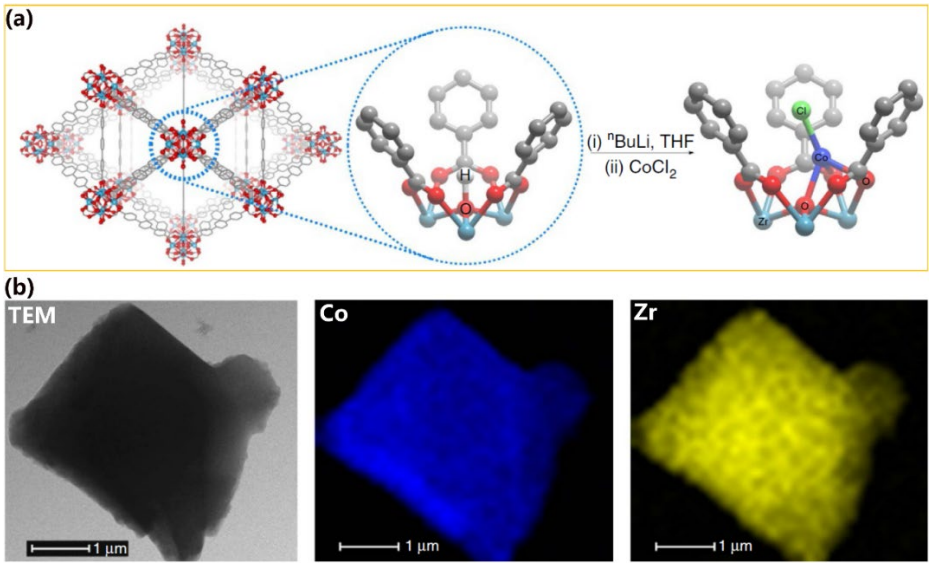

Figure 16. (a) Co-AIM metalation of MOF UiO-68 SBUs. (b) TEM-EDS mapping of UiO-68-Co. Reprinted with permission [160]. Copyright © 2016 Springer Nature Limited.

In the contribution of Manna and co-workers [160], they demonstrated a straightforward metalation of MOF UiO-68 by anchoring a single-site catalyst to the SBUs Zr-oxo clusters. As illustrated in Figure 16, the -OH groups that deprotonated by ^{n}BuLi reacted with $CoCl_2$ to yield Co-AIM UiO-68 MOF single-site solid catalysts, which exhibited excellent catalytic activities for organic reactions including silylation, chemo-selective borylation, benzylic C-H bonds amination, alkenes hydrogenation and ketones hydroboration. By following a similar approach, another single-site catalyst Zr-MTBC-CoH was also developed by first $CoCl_2$-metalating MOF Zr-MTBC and Hf-MTBC (MTBC = methanetetrakis *p*-biphenylcarboxylate), and subsequent treatment by $NaBEt_3H$. The derived catalysts displayed high activation and reusability for many hydrogenation reactions [161]. The mechanism studies indicated that chemo-selective organic transformations occurred on unsaturated metal centres, and AIM metalation has offered an option for catalysts engineering.

3.2.3. Nobel metals

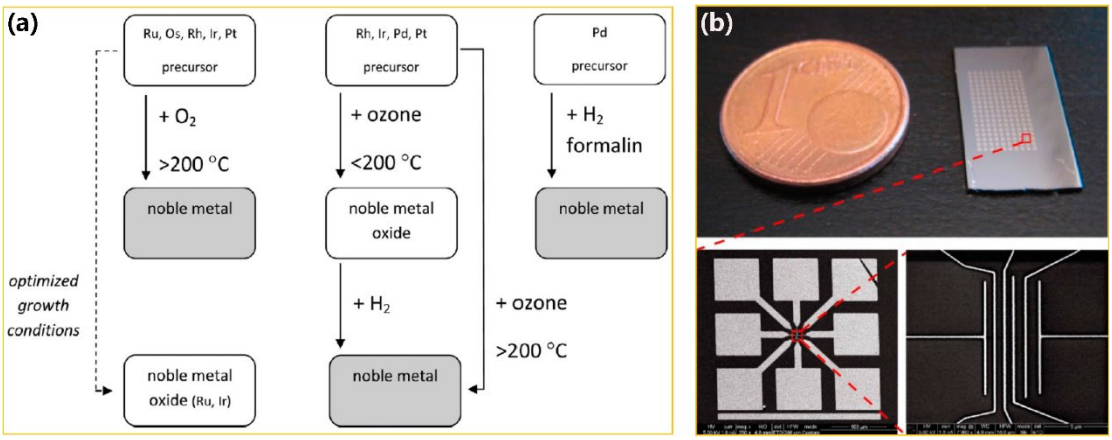

Figure 17. (a) ALD process to grow noble metal films. (b) ALD Al_2O_3-seeded patterning growth of Pt film. Reprinted with permission [162,163]. Copyright @ 2013 American Chemical Society.

As known, noble metals like palladium, silver, iridium, platinum, ruthenium, rhodium, osmium, and gold have good chemical resistance to various acids and oxidation. In some cases, it was desired to produce noble metal films. As shown in Figure 17, some work has demonstrated the feasibility by using ALD layer-seeded growth approach, and O_2 as a non-metal precursor to grow Pt films at temperature > 200 °C. In literature, Pd film could be derived at ALD processing temperatures < 200 °C and H_2 or O_3 as non-metal precursors. Apparently, O_3 and O_2 as ALD precursors tended to produce noble metal oxides. Besides, island growth rather than continuous layers was often observed at the beginning of the noble metal ALD processes, which could be advantageously used to disperse noble metal NPs onto MOFs crystals. Pt and Pd NPs with narrow size distributions have been successfully demonstrated by several research groups [164–

171]. Although MOFs as a scaffold offered the unique advantages in catalytic systems, AIM of noble metal has not been extensively explored yet.

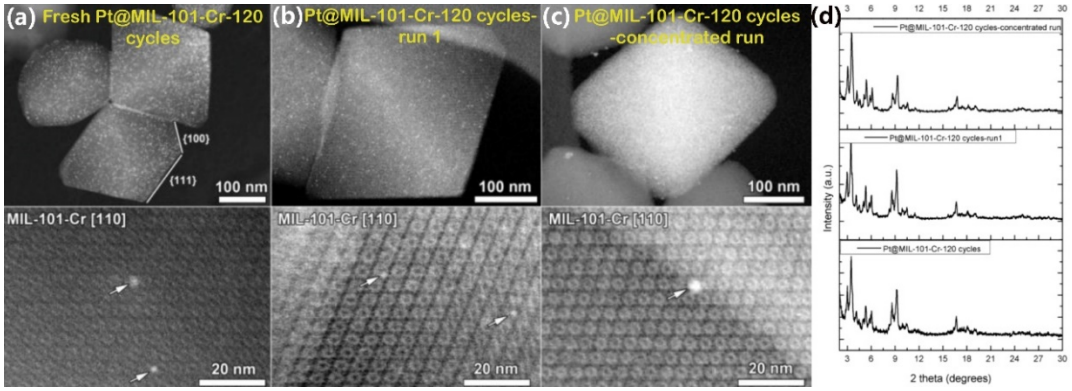

Figure 18. Top row: HAADF-STEM images, and bottom row: ADF-STEM images: Reprinted with permission [172]. Copyright © 2016 MDPI (Basel, Switzerland).

Pt-AIM MIL-101(Cr) was demonstrated by Leus et al. [172] to deposit Pt NPs into MOF MIL-101(Cr) structure using (methylcyclopentadienyl)-trimethyl platinum/O_3 ALD reaction system at 200 °C. In their experiments, different Pt loadings were achieved by changing the ALD cycling numbers, and the dimension of the MOF cages determined the sizes of the dispersed Pt NPs (Figure 18a–c). The porosity and crystallinity of MOF MIL-101 was well remained in the course of Pt NPs loading. Catalysed by the developed Pt@MIL-101-120 cycles catalyst, full conversion was achieved in olefins hydrogenation under mild reaction conditions. Stability tests with a long reaction time showed high stability of the developed catalysts (Figure 18d).

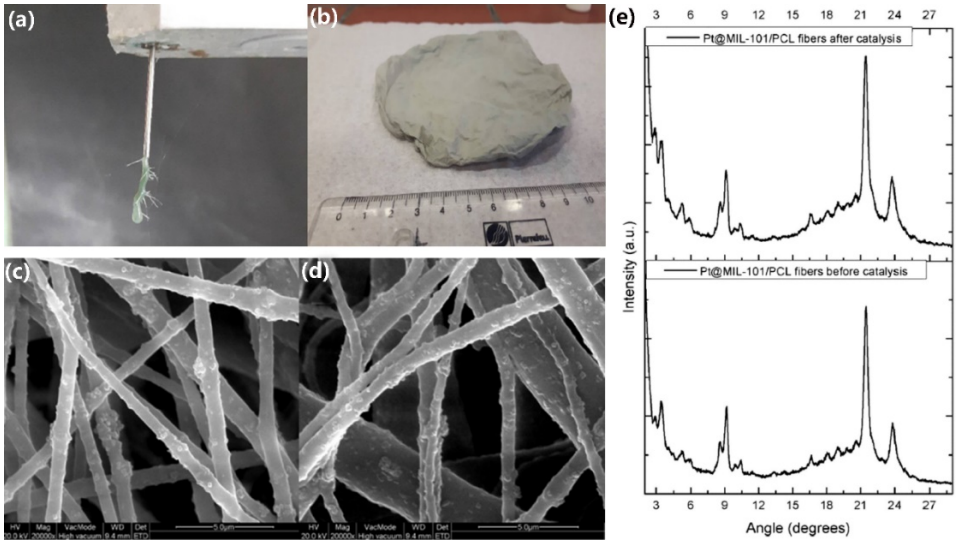

Figure 19. (a) A droplet in electrospinning process, (b) Catalytic carpet of Pt@MIL-101/PCL fibers, (c) as-electrospun catalytic carpet, (d) Catalytic carpet after 4 catalytic cycles, and (e) PXRD patterns of catalytic carpet before and after 4 catalytic cycles. Reprinted with permission [173]. Copyright © 2018 Elsevier Inc.

As a following-up work [173], a 'catalytic carpet' was created by electrospinning the Pt@MIL-101 nanoparticles containing poly-ϵ-caprolactone (PCL) matrix (Figure 19), and the carpet was proved to be active and robust in the cyclohexene hydrogenation. More importantly, the recovery of such 'catalytic carpet' could easily be realized after catalysis applications.

3.2.4. Theoretical studies

To better understand the dehydroxylation process during the post-synthetic modification of MOFs, Lemaire et al. [174] explored the site-specific reactions on how the commonly used ALD precursors such as TMA and titanium tetrachloride ($TiCl_4$) to dehydroxylate the example MOF UiO-66-NH_2. The real-time QCM and FTIR analysis showed that TMA and $TiCl_4$ reacted with not only μ_3-O and μ_3OH groups in the Zr_6-nodes, but also linkers within MOF UiO-66-NH_2 structure. Although these reactions were found to occur mainly around μ_3-OH hydroxyl sites on the MOF surface, $TiCl_4$ was found to penetrate into the subsurface of MOF crystals at a faster diffusion rate. FTIR spectroscopies revealed the reversible dihydroxylation of UiO-66-NH_2 by both TMA and $TiCl_4$ at 150 °C, and the distortion of Zr_6-clusters were noticed.

3.3. ALD deposition of MOFs films on target substrates

As known, although MOFs materials showed satisfactory results at small-scale trials, their powder forms in up-scaled applications remained questionable, for example, powder MOFs particles for water purification tended to develop high-pressure drop in a fixed adsorption bed, for catalysis reaction at an elevated temperature tended to aggregate, and for materials-based gas storage had the potential to block the pipelines in the charge/discharge cycles. Those matrix effects could be migrated by depositing MOF films onto the target surface as thin functional films or MOF membranes [175,176]. In literature, two ALD routes have been taken to deposit MOF films onto the target substrates. One route was to ALD deposit the metal and linker precursors first on the chosen substrates, and then post-deposition crystallization was conducted to grow MOF films via wet-based chemistry. In literature, this wet-based route found difficulty to work out with microelectronics and high aspect ratio structures, though the reaction conditions could be improved through optimization. Research Efforts were then made towards the gas-based chemistry for the post-deposition crystallization process. The other route was to deposit only metal precursors on the chosen substrates, and then the post-deposition crystallization of MOFs was conducted under the linker vapor environment.

3.3.1. Deposit metal/linker precursors and post-deposition crystallization

MOF-5 films were deposited by Salmi et al. [177] onto the target substrate at 225–350 °C by using zinc acetate ($ZnAc_2$) as metal precursor and 1,4-benzenedicarboxylic acid (1,4-BDC) as organic precursor. The as-prepared MOF-5 films showed X-ray amorphous and room temperature with humid conditions could crystallize them into an unknown crystalline phase,

but no porosity was observed from adsorption tests. The actual MOF-5 phase could be obtained when these films recrystallized in an autoclave at 150 °C containing vaporized dimethylformamide (DMF). Later, the same group [178] ALD deposited IRMOF-8 thin films at 260–320 °C by using 2,6-naphthalenedicarboxylic acid and zinc acetate as ALD precursors. Similarly, room temperature with 70% relative humidity conditions could crystallize the as-prepared amorphous films into an intermediate phase with large unit cells, and the DMF-contained autoclave could convert them into actual IRMOF-8. Although the properties of such MOF films prepared through wet-based chemistries could be tuned through the selection of linker molecules with different chemical groups, the wet-based processes presented difficulties to apply on microelectronics and high-aspect-ratio structures [179]. In this regard, all-gas-phase ALD technique with more advancements promised to solve the problems encountered in post-deposition crystallization process. For instance, Lausund et al. [180] deposited the thin amino-functionalized UiO-66 film through the ALD process using $ZrCl_4$ and 2-amino-1,4-BDC as precursors and then consecutive crystallization took place afterwards. In their experiments, the amino-functionalized BDC linkers showed better stoichiometry control over those unmodified ones, and modulators such as acetic acid were not required any more. The characterizations before and after crystallization confirmed the success of the crystallization of UiO-66 MOF thin films, and the functionalized UiO-66 exhibited hydrophilic character.

3.3.2. Deposit metal precursor and crystalize MOF films in ligand environment

Surface functionalization of inorganic NCs are important in the past practices, and the major difficulty was how to control the order of chemical reactions between different interfaces, so that different functional layers could be constructed in the desired order. In this regard, ALD process has displayed a better control by first depositing seeding layers onto the target substrate, and then growing MOF crystals on the seeding layers in liquid solutions [181–184]. Very often, the construction of core-shell hybrid would require a complex experimental design and the resulting MOF shells showed poor crystallinity and low dispersion [185]. To overcome this issue, Zhao et al. [186] proposed to arrange the well-defined MOF units in a spatial way, so as that the precise control over their textural properties could be achieved. In their demonstration, ALD Al_2O_3 film was firstly deposited on Ag nanocrystals, and then the hybrid of Ag NCs@ $[Al_2(OH)_2TCPP]$ MOF was obtained by exposing Ag NCs@ Al_2O_3 to the vapor 4,4',4'',4'''-(porphyrin-5,10,15,20-tetrayl) tetrabenzoic acid (H_4TCPP) linker. As shown in Figure 20, different thicknesses of Al_2O_3 films on the Ag NCs surfaces could be achieved by different ALD cycles, and $[Al_2(OH)_2TCPP]$ MOF films with thicknesses from 10 to 50 nm were achieved by precisely controlling the above Al_2O_3 film thickness from 0.1 to 3 nm. The crystallinities of MOF films and their orientations on Ag NCs surfaces could be controlled by the slow release rate of Al from Al_2O_3 layer. During their experiments, high crystalline $[Al_2(OH)_2TCPP]$ MOF

thin film with thickness of several nano-meters was made from the minimum ALD-deposited Al_2O_3 film with thickness <1 nm. The best quality [$Al_2(OH)_2TCPP$] MOF film was derived from the optimized solvent mixing ratio of water/DMF=3:1.

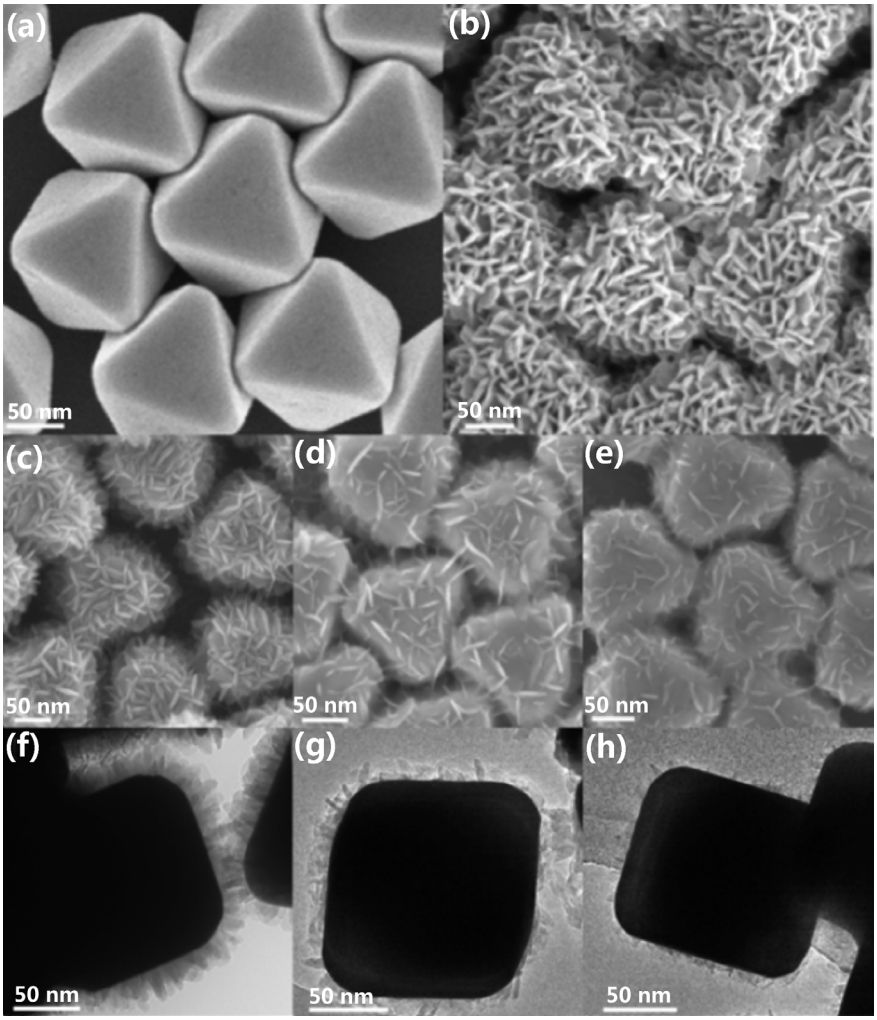

Figure 20. Electron microscopies of: (a) Ag NCs, (b) Ag NCs@ALD-Al_2O_3, (c,f) 3 nm thick ALD-Al_2O_3 on Ag NCs, (b,g) 0.5 nm thick ALD-Al_2O_3 on Ag NCs, and (e,h) 0.1 nm thick ALD-Al_2O_3 on Ag NCs. Reprinted with permission [186]. Copyright © 2015 American Chemical Society.

Vellingiri et al. [187] firstly coated titanium dioxide (TiO_2) films onto polyamide-6 nanofiber (PA-6) by ALD, and then a solvothermal growth method was applied to construct PA-6@TiO_2 MOF materials. George et al. [188] pioneered the growth of organic or hybrid organic-inorganic films by ALD using organic precursors or a combination of organic and inorganic precursors. This versatile work featured with the advantages offered by layer-by-layer method initiated other investigations by combining both methods to promote the growth of MOF on the fibers [189]. For instance, a nucleation layer of ALD-Al_2O_3 was first deposited onto cotton fibers by using 50 ALD cycles, and then subjected to 40 cycles of layer-by-layer (LBL) process to grow HKUST-1 ($Cu_3(BTC)_2$) crystalline onto the surface of cotton fibers/ALD-Al_2O_3 substrate. This

allowed to form a core@shell structure of cotton-Al_2O_3@MOF. Even though this technique ensured the preparation of cellulose@MOF composite with high content and homogenous distribution of MOFs, it was highly recommended to establish other amendable, time- and cost-effective approaches for industrial-scale production [190].

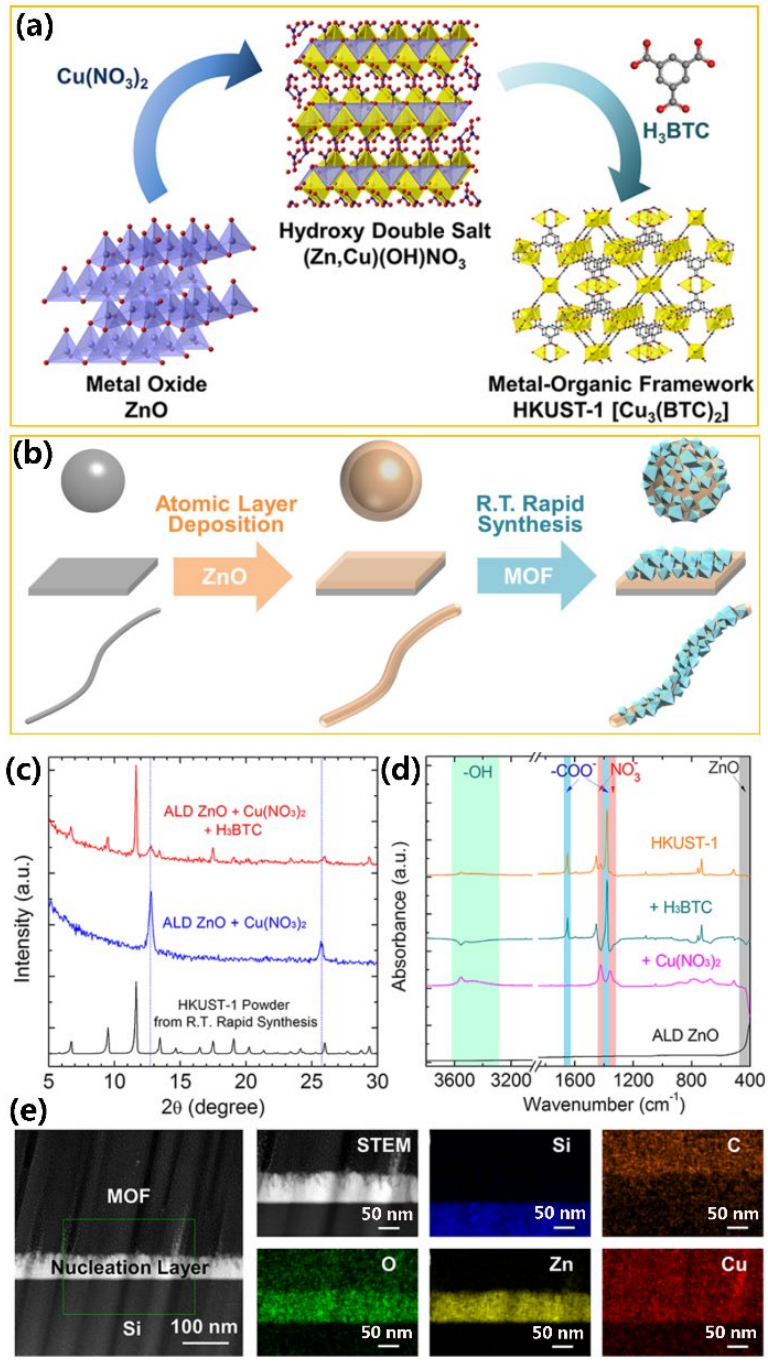

Figure 21. (a) Rapid HDS-assisted HKUST-1 synthesis at room-temperature, (b) HDS-assisted MOF films on different substrates, (c) XRD curves at each step of thesis, and the (Zn,Cu) HDS were indicated by the two dotted lines in blue. (d) FTIR spectra of samples at each step. (e) The cross-sectional view of Si/ALD deposited-ZnO/HKUST-1 MOF hybrid, and its HAADF-STEM as well as HR-EDX mapping images. Reprinted with permission [191]. Copyright © 2015 American Chemical Society.

As depicted in Figure 21, Zhao et al. [191] found that ALD-deposited ZnO films could react with $Cu(NO_3)_2$ into a hydroxy double salt (HDS) intermediate, which in turn induced the rapid formation of MOF HKUST-1 at room temperature within 1 min. As shown by the XRD curves in Figure 21c, the black curve represented the HKUST-1 powder as the reference. The other two curves recorded the rapid changes of XRD diffractions when the as-deposited ALD-ZnO sample reacted with $Cu(NO_3)_2$ (blue), and $Cu(NO_3)_2/H_3BTC$ (red), respectively. Wherein, the phase transitions of (Zn,Cu) HDS were highlighted by the two dashed lines in blue. In this approach, the fast anion-exchanges offered by (Zn,Cu) (HDS) intermediates promoted the rapid formation of MOF HKUST-1, and such synthetic generality was proved applicable to other MOF structures such as IRMOF-3, ZIF-8, and Cu-BDC. Besides, various substrate surfaces could be pre-patterned by ALD deposited-ZnO thin films, and dense HKUST-1 MOF coatings were demonstrated to grow onto different ALD pre-patterned substrates including silicon wafers, polymer spheres, and fibres. A high adsorption capacity for toxic gases was achieved in breakthrough tests by the MOF-functionalized fibers. With a space-time-yield (STY) up to 3×104 $kg/m^3 \cdot day$, such HDS-driven MOF synthesis approach could be highly feasible for MOF device integration, industrial implementation and commercialization.

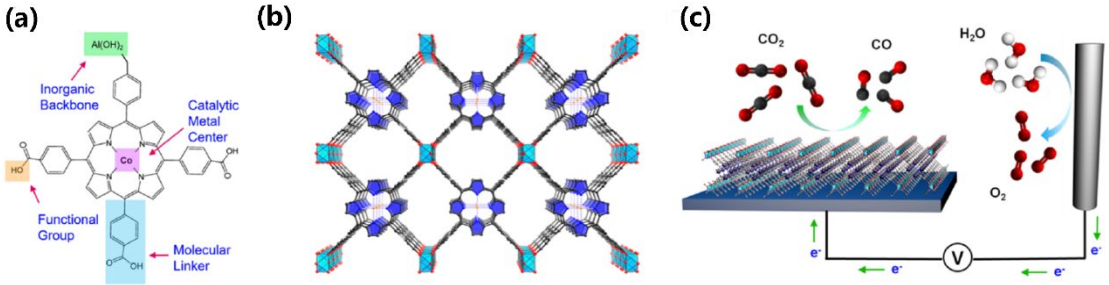

Figure 22. (a) MOF-integrated catalytic system provided a modular-level platform, (b) Assembled ALD-Co $Al_2(OH)_2TCPP$ MOF, (c) MOF-integrated catalytic system for aqueous CO_2 electrochemical reduction. Reprinted with permission [193]. Copyright © 2015 American Chemical Society.

One of the key factors for CO_2 electrochemical reduction practices was to design catalytic materials containing earth-abundant elements with high product selectivity and stability [192]. MOFs-based catalytic systems have been proposed by Kornienko et al. [193] to be modular platforms for CO_2 electrochemical reduction. In their investigation, MOFs were screened with systematically varied building blocks, and those with catalytic metal and linker units were selected and deposited onto conductive substrates (Figure 22). After the optimization of the MOF thickness, the ideal CO_2-reduction catalyst was obtained with good selectivity and stability toward CO production. Such modular systems provided opportunities for further improved performance in electrocatalysis.

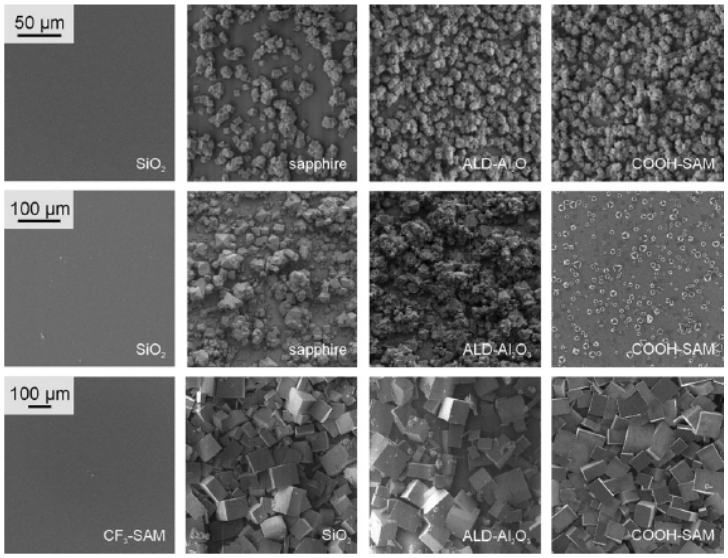

Figure 23. ALD Al_2O_3 layer-assisted coating of MOF-5 onto sapphire substrate. Reprinted with permission [194]. Copyright © 2007 American Chemical Society.

Hermes et al. [194] successfully coated c-plane (0001) sapphire with ALD-Al_2O_3 amorphous films, and afterwards MOF-5 crystalline films were grown densely on the basis of the buffing ALD-Al_2O_3 films (Figure 23). However, the authors failed to deposit MOF-5 films on SiO_2 substrates by following the same strategy, and the poor film adhesive ability might account for this failure [195,196]. An alumium-porphyrin-based MOF-55 was employed by Kornienko et al. [197] for the electrocatalytic reduction of CO_2 into CO. In their study, a thin film of ALD-Al_2O_3 was deposited as a metal precursor, and then reacted with the linker under solvothermal conditions to form MOF films. The desired thickness of MOF catalytic films was eventually achieved through tuning the number of ALD precursor-depositing cycles. The improved performance of the resulting MOF catalyst was achieved with increasing MOF film thickness, which indicated a trade-off between electron and mass transport [198].

In literature, although UiO-66-NH_2 as highly tuneable MOF has been proved to be an effective catalyst to degrade chemical warfare agents (CWAs) with a half-life of 1 min, its powder form limits its deployment opportunities. To respond this, many researchers adopted LBL approach with slow solvothermal synthesis to produce supported MOF materials for improved application efficiency, and MOFs-coated polymer fibers would facilitate the further device integrations towards the envisioned applications. In this area, fibrous composites were synthesized in an attempt to transform the powder MOFs into an application-oriented structure. Recent progress has been indicated that well-adhered MOF films could be grown on the ALD pre-conditioned surfaces of the target substrates. Several important work from Pasons group [199–207] can be referred by following the timeline.

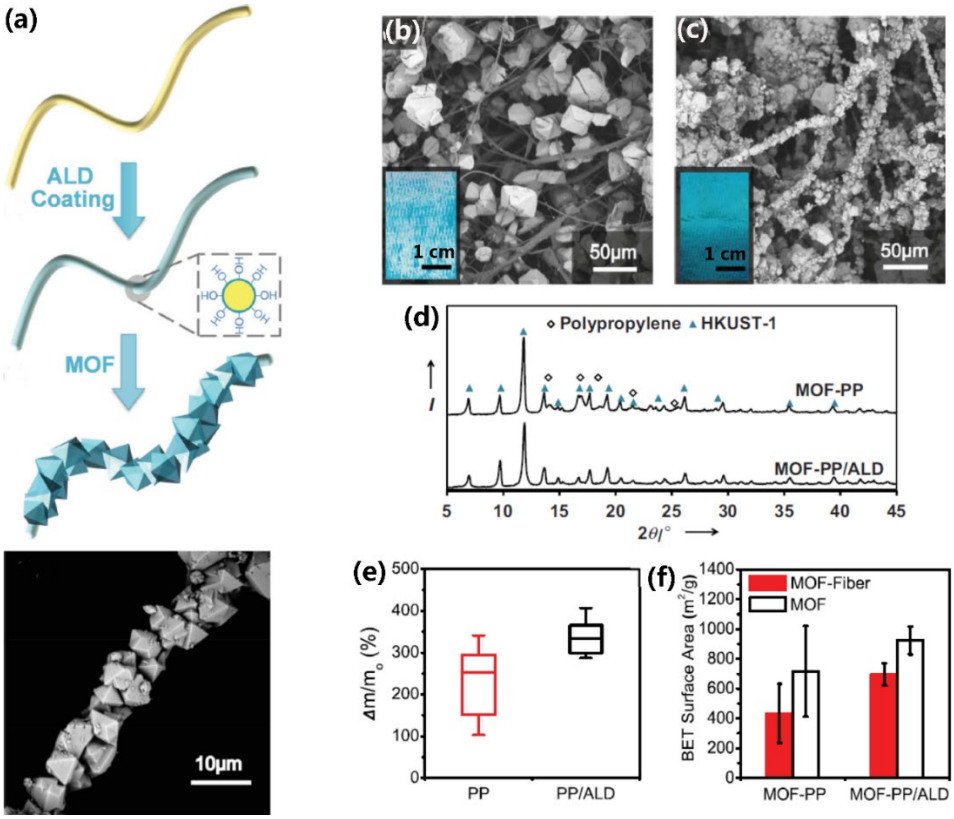

Figure 24. (a) MOF growth on ALD-coated polymer fibers, (b) HKUST-1 MOF/untreated PP fiber, (c) HKUST-1 MOF/ALD Al_2O_3-coated PP fiber, (d) XRD patterns of HKUSI-1/PP and HKUSI-1/ALD-PP, (e) Different HKUSI-1 MOF mass loadings, and (f) BET surface areas. Reprinted with permission [199]. Copyright © 2014 WILEY-VCH Verlag GmbH & Co. KGaA, Weinheim.

Their work published in 2014 [199] loaded MOFs with large surface areas on fibrous materials to achieve high adsorptive capacities. Figure 24 illustrated the synthesis scheme to grow MOF crystals onto the polypropylene (PP) fibers precoated by ALD-Al_2O_3 for 200 cycles at 60 °C. On one hand, the hydroxyl groups on the PP@ALD-Al_2O_3 surface changed the wettability of PP fibers for a better permeation of solvothermal solvents, and preconditioned the PP surface to load MOF crystals. On the other hand, MOF nucleation could be also promoted by the increased surface roughness from the grown ALD-Al_2O_3 coatings on the PP fibers. As an example, PP fibers were precoated with ALD-Al_2O_3 by using $Cu(NO_3)_3 \cdot 3H_2O$ and BTC acid as precursors, and HKUST-1 MOF was solvothermal grown onto ALD precoated PP at 120 °C in the mixed solution of water/ethanol (50/50 vol%) for 20 h. The characterization results indicated that the functionalities of HKUST-1 MOF remained unchanged, and good adhesion of MOF crystals were achieved to the PP fibers. The authors also applied this approach to other similar substrates such as cotton and PET, and other MOFs such as MOF-74 and UiO-66 [200,201]. As introduced earlier, their work published in 2015 [191] reported ALD-formed HDS film to yield dense and strongly adhered MOF Cu-TCPP on fibres without aggregation,

which otherwise would lead to poor adhesion to substrates. In comparison with MOF powders, the resulting fiber@MOF composite exhibited 3× higher NH_3 adsorptive capacity and a nearly retained 2-chloroethyl ethyl sulphide (CEES) adsorptive capacity in humid conditions.

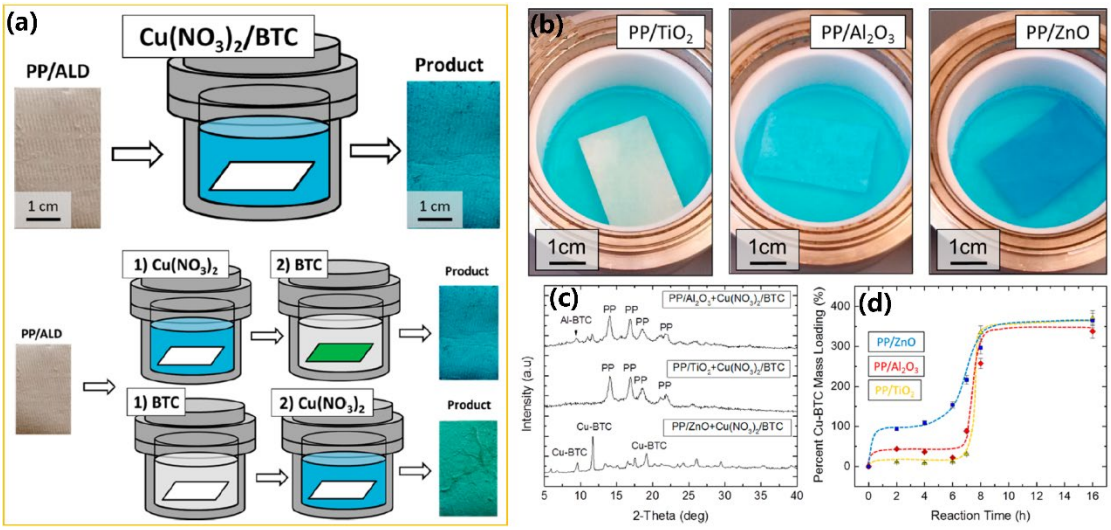

Figure 25. (a) The used process to grow Cu-BTC on the target substrate. (b) Photos of Cu-BTC nucleation on PP/ALD, (c) XRD patterns recorded the rapid Cu-BTC nucleation, and (d) The mass loadings of Cu-BTC on different PP/ALD substrates. Reprinted with permission [202]. Copyright © 2016 American Chemical Society.

In 2016 [202], they developed a method (Figure 25) to construct MOF-nanofiber kebabs on ALD-treated Nylon-6 nanofibers. As recorded by XRD patterns in Figure 25c, a rapid room temperature nucleation of Cu-BTC MOF could be observed on PP/ZnO sample. With an early initial mass loading on the target substrates, the white PP/ZnO sample changed rapidly to blue color. The ALD-deposited TiO_2, Al_2O_3 and ZnO layers promoted the solvothermal growth Cu-BTC on those ALD-treated substrate surfaces. In their experiments, solvothermal Cu-BTC nucleation took place on ALD-treated PP substrates at room temperature, and the ALD-deposited metal layers affected the speed of MOF nucleation time and the textual properties of the resulting materials. Their work published in 2017 [203] assembled pre-synthesized UiO-66-NH_2 MOF crystals onto ALD-preconditioned PP mats and obtained the so-called catalytic 'MOF-cloth' (Figure 26). In their study, the PP fibrous mats were pre-conditioned using ALD conformal metal oxide (Al_2O_3, TiO_2, or ZnO) thin films, and the hydrophilic nature of those metal oxide surfaces facilitated the good coverage and high-loaded MOF up to 40 wt. %. The assembly of UiO-66-NH_2 MOF crystals were chemically directed by two surfactants of cetyltrimethylammonium bromide (CTAB) and βcyclodextrin (β-CD). It's worthy to mention that those two rapidly self-assembled agents not only impeded the MOFs nucleation in the solution, but also promoted strong adhesion of MOF crystals to the surface. The best sample

with BET surface area of 200 m^2/g achieved a half-life < 5 min in the catalytic degradation of CWA simulant dimethyl 4-nitrophenyl phosphate (DMNP).

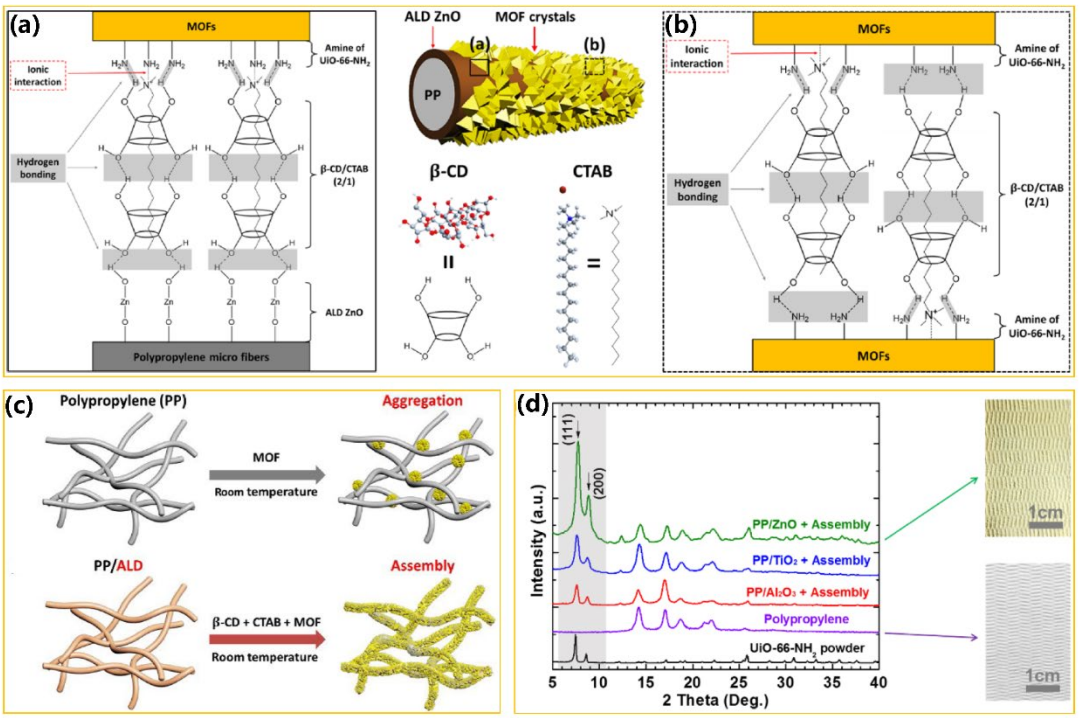

Figure 26. (a) Ionic interactions allowed pre-synthesized UiO-66-NH_2 MOF grown on ALD pre-conditioned PP fibers, (b) Loaded UiO-66-NH_2 MOF crystals with different structures, (c) ALD pre-condition of substrate facilitated MOFs growth, and (d) XRD patterns with sample photos on the right side. Reprinted with permission [203]. Copyright © 2017 American Chemical Society.

Note that the good adhesion of a favorable MOF such as UiO-66 (Zr) to the polymer substrates could be achieved by ALD pre-deposition of a metal oxide film onto the target substrates before the growth of MOF. Lee et al. [204] explored how different ALD-deposited nucleation films (TiO_2, ZnO, or Al_2O_3) would influence the quality of grown UiO-66-NH_2 MOF films and their adhesion to the target substrates. As shown in Figure 27, out of the three nucleation films explored, ALD-TiO_2 film was found to yield the strongest fiber@UiO-66-NH_2 MOF adhesion, and ALD-ZnO film however induced a higher mass loading of UiO-66-NH_2 MOF on target PP mats. The Zn^{2+} ions from chemically instable ALD-ZnO film was believed to facilitate the homogeneous growth of UiO-66-NH_2 MOF films.

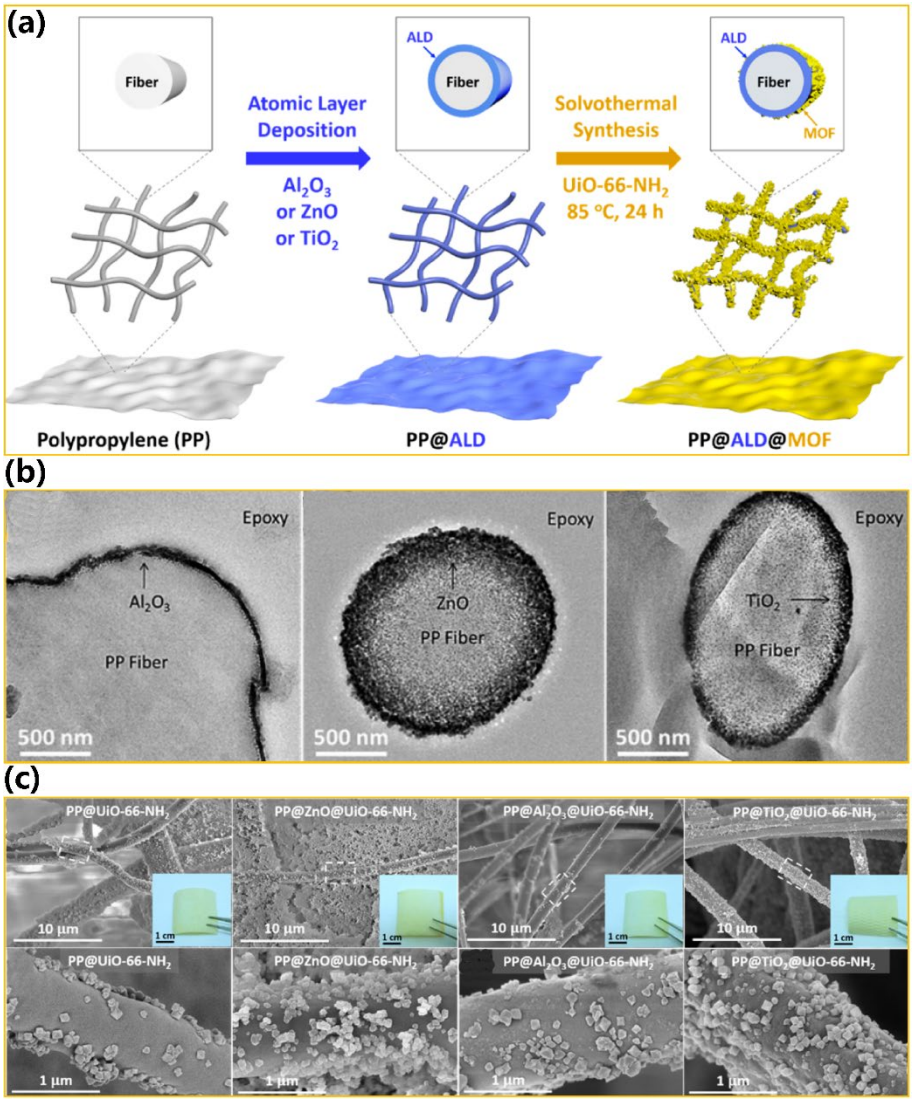

Figure 27. (a) Pre-condition and grow MOF UiO-66-NH_2 onto fiber substrates, (b) TEM images of PP@Al_2O_3, PP@ZnO, and PP@TiO_2 samples, and (c) MOF UiO-66-NH_2 crystalline grown on PP, PP@ZnO, PP@Al_2O_3, and PP@TiO_2 (actual photos inserted). Reprinted with permission [200]. Copyright © 2017 American Chemical Society.

In 2018 [205], they reported MOF growth onto different ALD-TiO_2 treated composite fibers via solvothermal synthesis (Figure 28). There were no obvious morphological changes before and after ALD-deposited TiO_2 films on the fiber substrates. After solvothermal synthesis, there was very little MOF crystals grown on substrate PVDF/$Ti(OH)_4$@TiO_2, while other three substrates of PP@TiO_2, PA-6@TiO_2 and PMMA/$Ti(OH)_4$@TiO_2 gained good coverages of MOF crystals. The Ti-F interaction occurred between ALD-TiO_2 and PVDF was responsible for the poor MOF growth on the PVDF composite, and the catalytic activities of the obtained composites on toxic organophosphate hydrolysis were found to rely on mass loadings of the active MOF crystals.

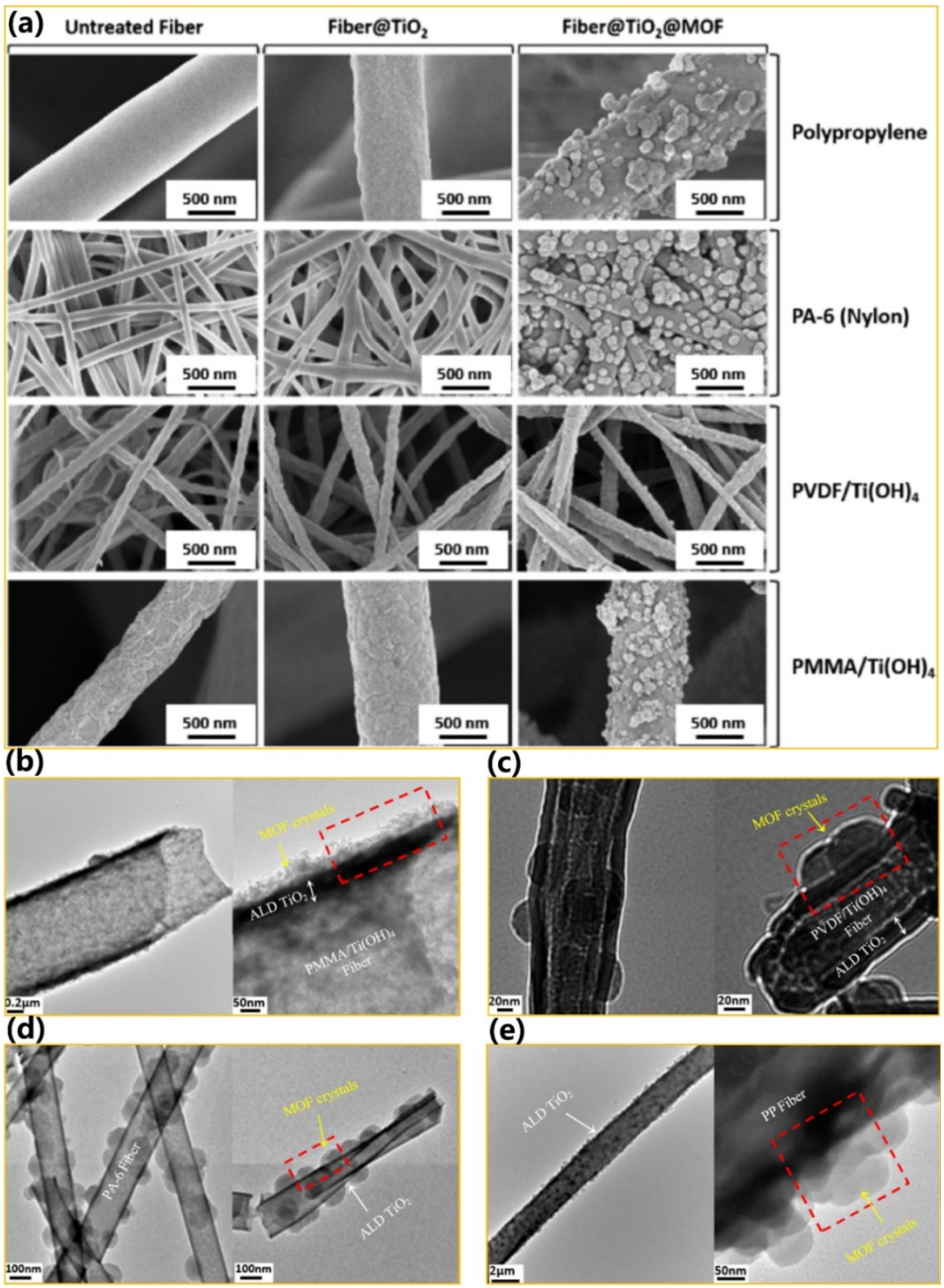

Figure 28. (a) Different fiber substrates. (b-e) TEM images showing MOF growth on different ALD-TiO_2 treated fiber substrates. Reprinted with permission [205]. Copyright © 2018 American Chemical Society.

As illustrated in Figure 29, Lee et al. [206] in 2019 reported a facile strategy to fabricate protective PP@Zn-TCPP textiles. In their studies, the PP fibers was first pre-treated with ~20 nm thick ALD-ZnO film, and then put under TCPP linker environment to convert ALD-ZnO films to Zn-TCPP MOF (40 °C, 12 h). Two alternative routes were demonstrated to obtain PP@Cu-TCPP composite: (i) exposed PP@ZnO to $Cu(NO_3)_2$ and TCPP (40 °C, 12 h), and (ii) converted ALD-deposited ZnO to HDS(Zn,Cu) in $Cu(NO_3)_2$ solution (25 °C, 2 min), and subsequent anion exchange with TCPP (40 °C, 12 h) formed PP@Cu-TCPP composite. Usually,

poor distribution and adhesion of MOF crystals on the fiber mats were observed through the conventional method. While good distribution and strong adhesion were achieved through the HDS(Zn,Cu) approach as discussed in the earlier time. Although bonding force was not readily measurable, the strong adhesion was tested by physical brushing the samples and good water stability of PP@Cu-TCPP composites was proved by hydrolysis tests. Besides, it was also possible to make PP@mixed Co/Zn-TCPP MOF hybrid. NH_3 adsorption tests on the best hybrid sample under wet conditions exhibited 3 times higher capacity than that of MOF powder. Such approach showed the potentials to make smart textiles.

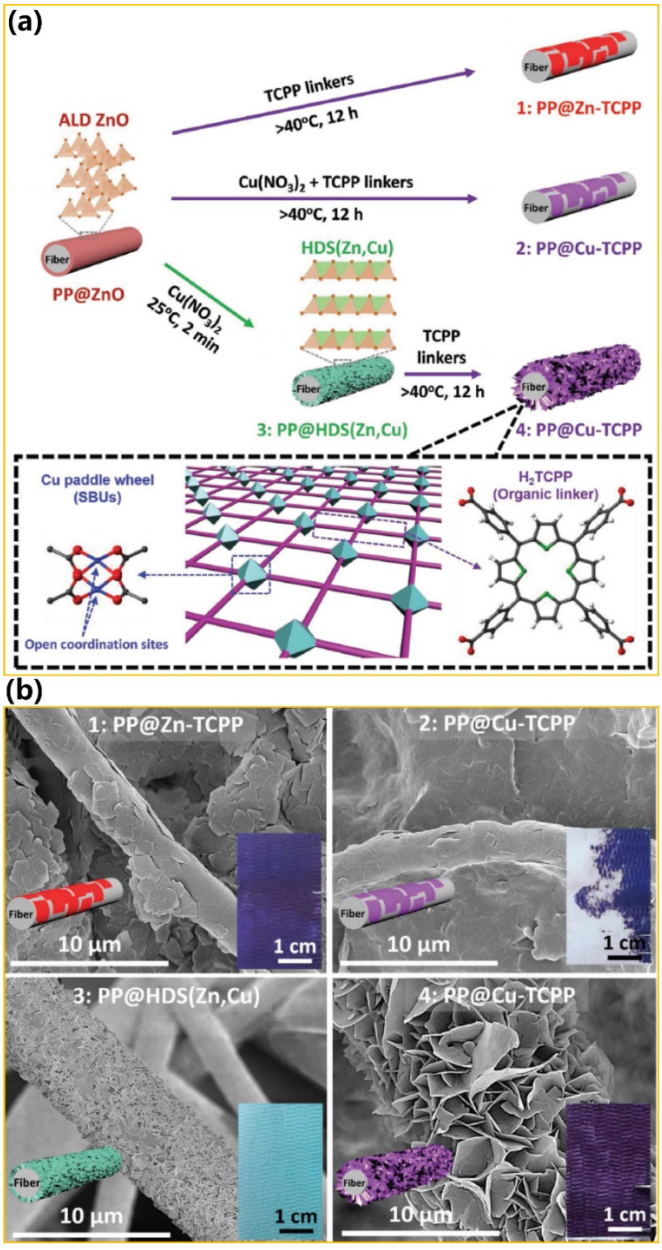

Figure 29. (a) Different routes to make PP@Co/Zn-TCPP MOF composites, (b) SEM images of the resultant four composites (actual photos inserted). Reprinted with permission [206]. Copyright © 2019 WILEY-VCH Verlag GmbH & Co. KGaA, Weinheim.

A recent work published in 2020 [207] investigated the effects of different ALD pre-deposited metal oxide films on the nucleation processes of MOF films, and probed the suitable synthesis mechanism for each of the metal oxide sources (Figure 30). In their experiments, different hydroxylation level of the studied ALD Al_2O_3, TiO_2 and ZnO films was isolated as an indicator to tell whether the ALD deposited metal oxide thin films served to promote the nucleation or they tended to convert straightforward to MOF crystallites. The results recognized that although the hydroxylation of ALD metal oxides was crucial to promote MOF nucleation, the fully pre-hydroxylated metal oxides films exhibited the loss of reactivity due to the water molecules physiosorbed. In other words, a metal reactant in its hydration state with trace of water would promote its film hydrolysis and in turn facilitate MOF nucleation. Later, MOF-525 was demonstrated to grow on ALD-Al_2O_3, ALD-ZnO, and ALD-TiO_2 coated fibers, wherein the ALD Al_2O_3-coated sample gained less MOF-525 growth and exhibited a slower rate to degrade DMNP.

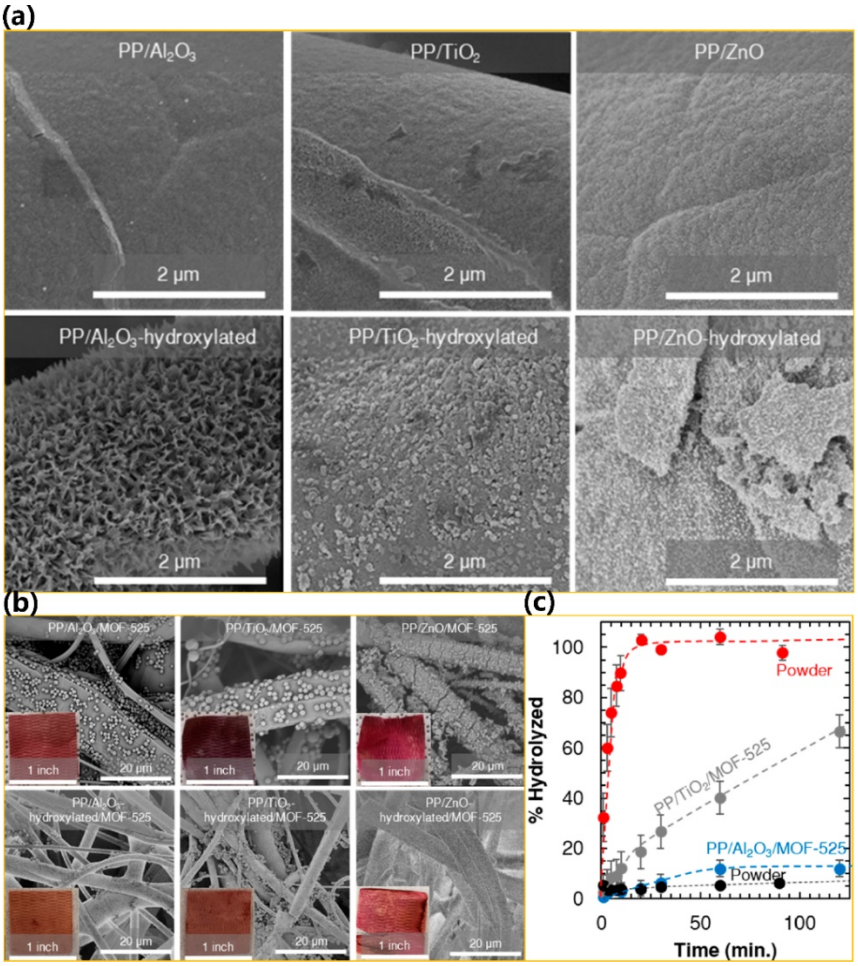

Figure 30. (a) SEM images of different pre-conditioned PP substrates, (b) MOF-525 growth on different pre-conditioned PP substrates, and (c) Performance comparison of DMNP hydrolysis. Reprinted with permission [207]. Copyright © 2020 American Chemical Society.

3.4. Theoretical studies

TMA, diethylzinc, and $TiCl_4$ have been commonly used as ALD precursors, their interaction with water in the ALD deposition process must be derived from in-situ characterization and well understood before any optimizations could be implemented effectively. A combined analysis including in-situ XPS, IR, and ab initio calculations were conducted by Tan et al. [208] to probe their interactions with other groups. In their study, H_2O and OH groups within several Zr-MOF structures were particularly focused on their reactivity dependences on the structural and chemical conditions. They found that the reactivities of OH groups were subject to their location, chemical environment, and accessibility in the Zr_6-nodes. For instance, given three typical MOFs of MOF-808, Zr-abtc, and UiO-66-NH_2, the activation temperatures for OH groups within their Zr_6-clusters to react with TMA were 24, 150, and 200 °C, respectively, which increased with the decreasing node connectivity. In contrast, no reactions were observed between the OH groups within Zr_6-clusters of UiO-66 MOF structure and TMA. The Ab initio calculations indicated that the functional NH_2 group near the target OH group directly catalyzed the reaction by anchoring the TMA molecule effectively. Meanwhile, it was found that the H_2O adsorbed on the MOF crystals would react with TMA easily at room temperature to form a thick Al_2O_3 film. Apparently, the uniform ALD-film deposition onto MOF crystals would necessitate the measures to uniformly distribute reactive −OH groups in each MOF node within the target MOF structure, as usually the ALD species were observed to preferentially deposited in some MOF pores.

While the organometallic precursor presumably tends to diffuse and react through the large MOF channels, after ALD treatments in some studies, new electron density was also observed in the small pores. No doubt, such selective deposition on only half available reaction sites were responsible for the poor film distributions in an ALD-deposition process. Through real-time ALD-XRD, Gallington et al. [209] visualized the localization and redistribution of the ALD-deposited atoms within the MOF NU-1000(Zr) structure. The deposition was observed to rather occur in the small cavities between the neighboring channels than in the channels with more accessibilities, and the sizes of used ALD precursors may also influence this regioselectivity. The authors pointed that such phenomenon was caused by the preferential adsorption of chosen ALD precursors on the MOF reactive sites. Similar evidence was found by Liu et al. [210] who examined the relations between pocket sizes and adsorption energies of ALD precursor $Zn(Et)_2$ on Zr_6-nodes within the substituted NU-1000(Zr) MOF structure. The results showed that the shorter distances between benzene groups and ALD precursors in the small pores allowed stronger interactions. More substitutions within NU-1000(Zr) MOF structure would create more shorter distances in the large pore to accommodate ALD precursors, which would re-balance the dispersion of favorable sites between large and small pores. All the above findings

could guide the AIM design process towards the desired characteristics of the MOFs-enabled device integrations.

4. Conclusions

Metal-organic frameworks (MOFs) has been thought to be magic powers with unlimited applications. Their powder forms, however, limit their wide utilization in the actual practices. Depending on the requirements from envisioned applications, MOFs sometimes are desired to serve various purposes with suitable functionalities, or themselves to be integrated as MOFs films into different devices. ALD is the capable technique of choice to deposit high-quality material films uniformly on MOF powders, or grow MOFs films directly on the target substrates. The overview from the literature on the current technology readiness level (TRLs) of MOFs technologies indicated the up-to-date MOFs research, development, and innovation (RD&I) are still sitting between TRL3 and TRL4. Taking technology from laboratory pieces to device integration is always a challenge, and their progression towards higher TRLs needs the collective advancements from other technologies. ALD has been introduced in the past two decades as a truly enabling technology and expected to assist the visibility of MOFs technologies by facilitating the MOFs devices integration.

This review brought together the scattered literature that addresses the past ALD research efforts towards MOFs films growth, post-synthetic functionalization, and devices integration. Firstly, several important advancements for MOFs device integration including MOFs surface preparation and defect engineering, MOFs pore size distribution, all gas-phase techniques for deposition of MOFs films, scaling-up solutions, essential characterization techniques for ALD MOFs films as well as toxicity evaluation on MOFs device integration. Then, the relevant ALD practices for MOFs devices integration were reviewed including ALD post-synthetic functionalization of MOFs, ALD confinement of nanocatalysts into MOFs, ALD deposition of MOFs films on target substrates and theoretical studies. In the context, the parallel advancements such as lessons or concepts from other technologies to be beneficial were also drawn to guide further optimization and improvement of applications based on MOFs-enabled technologies. Compare to the liquid-phase MOF thin-film approaches for microelectronics industries, ALD-based techniques firstly provide more convenience to control the reagents spatiotemporally. Secondly, they avoid surface-tension phenomena and the possible corrosion of the electronic devices by requiring no solvents. Thirdly, ALD-based techniques provide the higher chance to scale-up and work on substrates with larger areas for MOF thin-film deposition. Although the heating of the precursors are usually necessary to improve the ALD reaction kinetics, and the applied temperature may cause problems for the thermally sensitive organic

compounds, the intensive developments on ALD precursors, processes and reactors can be expected to mitigate this negative impact shortly. Finally, it is noted that the combination of MOFs with ALD processing technique is crucial for the possible MOFs device integration. However, the short answer to the question of 'when will the MOFs-integrated devices to become widely available' is 'This would take a while'. As it is very difficult for a new technology to replace the existing technologies on the market in a short time. It will be much more likely that new areas or problems where no solutions existing before the discovery of MOFs or a combination of MOFs with other materials for better performance. Irrespective of which device will be the first to introduce MOFs and commercialized, ALD will likely play an import role to bring them into reality.

Acknowledgement

The financial supports from South African National Research Foundation (NRF) for research activities under the South Africa/Poland joint collaboration grant (grant no.: 118676) are highly acknowledged.

References

[1] A.U. Czaja, N. Trukhan, U. Müller, Chem. Soc. Rev. 38 (2009) 1284−1293.

[2] R.F. Service, Science 346 (2014) 538−541.

[3] J.W. Ren, X. Dyosiba, N.M. Musyoka, H.W. Langmi, M. Mathe, S.J. Liao, Coord. Chem. Rev. 352 (2017) 187−219.

[4] F. Trapani, A. Polyzoidis, S. Loebbecke, C.G. Piscopo, Micropor. Mesopor. Mater. 230 (2016) 20−24.

[5] H. Kim, S. Yang, S.R. Rao, S. Narayanan, E.A. Kapustin, H. Furukawa, A.S. Umans, O.M. Yaghi, E.N. Wang, Science 356 (2017) 430−434.

[6] H. Kim, S.R. Rao, E.A. Kapustin, L. Zhao, S. Yang, O.M. Yaghi, E.N. Wang, Nat. Commun. 9 (2018) 1191.

[7] F. Meunier, Science 358 (2017), eaao0361.

[8] W.L. Queen, ACS Cent. Sci. 3 (2017) 531−532.

[9] M.J. Kalmutzki, C.S. Diercks, O.M. Yaghi, Adv. Mater. 30 (2018) 1704304.

[10] R.W. Johnson, A. Hultqvist, S.F. Bent, Mater. Today, 17 (2014) 236−246.

[11] T. Faraz, F. Roozeboom, H.C.M. Knoops, W.M.M. Kessels, ECS J. Solid State Sci. Tech. 4 (2015) N5023−N5032.

[12] R.L. Puurunen, Chem. Vap. Depos. 20 (2014) 332−344.

[13] E. Alvaro, A. Yanguas-Gil, PLoS ONE 13 (2018) e0189137.

[14] T.J. Knisley, L.C. Kalutarage, C.H. Winter, Coord. Chem. Rev. 257 (2013) 3222−3231.

[15] A. Devi, Coord. Chem. Rev. 257 (2013) 3332−3384.

[16] G.Y. Fang, L.N. Xu, Y.Q. Cao, A.D. Li, Coord. Chem. Rev. 322 (2016) 94−103.

[17] S.W. Lee, B. J. Choi, T. Eom, J.H. Han, S.K. Kim, S.J. Song, W. Lee, C.S. Hwang, Coord. Chem. Rev. 257 (2013) 3154−3176.

[18] K.B. Ramos, M.J. Saly, Y.J. Chabal, Coord. Chem. Rev. 257 (2013) 3271−3281.

[19] A.C. Johanson, J.D. Parish, Recent developments in molecular precursors for atomic layer deposition, in Organometallic Chemistry: Volume 42, 2018, pp. 1−53

[20] F. Zaera, Coord. Chem. Rev. 257 (2013) 3177−3191.

[21] S.M. George, Chem. Rev. 110 (2010) 111−131.

[22] S.T. Barry, Coord. Chem. Rev. 257 (2013) 3192−3201.

[23] V. Cremers, R.L. Puurunen, J. Dendooven, Appl. Phys. Rev. 6 (2019), 021302.

[24] D. Muñoz-Rojas, V.H. Nguyen, C.M. de la Huerta, S. Aghazadehchors, C. Jiménez, D. Bellet, C. R. Phys. 18 (2017) 391−400.

[25] S.E. Potts, W.M.M. Kessels, Coord. Chem. Rev. 257 (2013) 3254−3270.

[26] H. Yan, H. Cheng, H. Yi, Y. Lin, T. Yao, C.L. Wang, J.J. Li, S.Q. Wei, J.L. Lu, J. Am. Chem. Soc. 137 (2015) 10484−10487.

[27] Z.H. Weng, F. Zaera, Top. Catal. 62 (2019) 838−848.

[28] L.Y. Wen, M. Zhou, C.L. Wang, Y. Mi, Y. Lei, Adv. Energy Mater. 6 (2016) 1600468.

[29] A.R. Pascoe, L. Bourgeois, N.W. Duffy, W.C. Xiang, Y.B. Cheng, J. Phys. Chem. C 117 (2013) 25118−25126.

[30] S. Seong, I.S. Park, Y.C. Jung, T. Lee, S.Y. Kim, S.J. Lee, J. Ahn, Electron. Mater. Lett. 15 (2019) 493−499.

[31] J. Ahn, C. Ahn, S. Jeon, J. Park, Appl. Sci. 9 (2019) 1990.

[32] G.N. Parsons, S.E. Atanasov, E.C. Dandley, C.K. Devine, B. Gong, J.S. Jur, K. Lee, C.J. Oldham, Q. Peng, J.C. Spagnola, P.S. Williams, Coord. Chem. Rev. 257 (2013) 3323−3331.

[33] C. Marichy, N. Pinna, Coord. Chem. Rev. 257 (2013) 3232−3253.

[34] R.H.J. Vervuurt, W.M.M. Kessels, A.A. Bol, Adv. Mater. Interf. 4 (2017) 1700232.

[35] C.J. Brinker, G.W. Scherer. Sol-Gel Science, Academic Press, San Dieto, CA, 1990.

[36] C. Powell, J. Mater. Res. 121 (1997) 557.

[37] D.M. King, X.H. Liang, A.W. Weimer, Powder Tech. 221 (2012) 13−25.

[38] P.O. Oviroh, R. Akbarzadeh, D.Q. Pan, R.A.M. Coetzee, T.C. Jen, Sci. Tech. Adv. Mater. 20 (2020) 465−496.

[39] V. Miikkulainen, M. Leskelä, M. Ritala, R. L. Puurunen, J. Appl. Phys. 113 (2013) 021201.

[40] B.J. O'Neill, D.H.K. Jackson, J. Lee, C. Canlas, P.C. Stair, C.L. Marshall, J.W. Elam, T.F. Kuech, J.A. Dumesic, G.W. Huber, ACS Catal. 5 (2015) 1804−1825.

[41] H. Kim, H. Lee, W.J. Maeng, Thin Solid Films 517 (2009) 2564−2580.

[42] N. Sobel, C. Hess, Angew. Chem. Int. Ed. 54 (2015) 15014−15021.

[43] J.W. Elam, M.D. Groner, S.M. George, Rev. Sci. Instrum. 73 (2002) 2981−2987.

[44] J.D. Ferguson, A.W. Weimer, S.M. George, Chem. Mater. 12 (2000) 3472−3480.

[45] D.M. King, J.A. Spencer, X.H. Liang, L.F. Hakim, A.W. Weimer, Surf. Coat. Tech. 201 (2007) 9163−9171.

[46] J.R. Wank, S.M. George, A.W. Weimer, Powder Tech. 121 (2001) 195−204.

[47] O.J. Kilbury, K.S. Barrett, X. Fu, J. Yin, D.S. Dinair, C.J. Gump, A.W. Weimer, D.M. King, Powder Tech. 221 (2012) 26−35.

[48] A. Kidanemariam, J. Lee, J. Park, Polymers 11 (2019) 2090.

[49] K. Leus, J. Dendooven, N. Tahir, R. Ramachandran, M. Meledina, S. Turner, G. Van Tendeloo, J. Goeman, J. Van der Eycken, C. Detavernier, P. van der Voort, Nanomaterials 6 (2016) 45.

[50] J.E. Mondloch, M.J. Katz, W.C. Isley III, P. Ghosh, P. Liao, W. Bury, G.W. Wagner, M.G. Hall, J.B. DeCoste, G.W. Peterson, R.Q. Snurr, C.J. Cramer, J.T. Hupp, O.K. Farha, Nat. Mater. 14 (2015) 512−516.

[51] Y. Wang, W.Z. Zhang, X.M. Wu, C.Y. Luo, T. Liang, G. Yan, J. Magn. Magn. Mater. 416 (2016) 226−230.

[52] J.W. Ren, N.M. Musyoka, H.W. Langmi, J. Walker, M. Mathe, S.J. Liao, Polyhedron, 153 (2018) 205−212.

[53] A.W. Thornton, R. Babarao, A. Jain, F. Trousseletn, F.X. Coudert, Dalton Trans. 45 (2016) 4352−4359.

[54] Z.L. Fang, B. Bueken, D.E. De Vos, R.A. Fischer, Angew. Chem. Int. Ed. 54 (2015) 7234−7255.

[55] D.S. Sholl, R.P. Lively, J. Phys. Chem. Lett. 6 (2015) 3437−3444.

[56] J.W. Ren, M. Ledwaba, N. Musyoka, H. Langmi, M. Mathe, S. Liao, W. Pang,

Coord. Chem. Rev. 349 (2017) 169−197.

[57] L.Y. Yuan, M. Tian, J.H. Lan, X.Z. Cao, X.L. Wang, Z.F. Chai, J.K. Gibson, W.Q. Shi, Chem. Commun. 54 (2018) 370–373.

[58] C. Crivello, S. Sevim, O. Graniel, C. Franco, S. Pané, J. Puigmartí-Luis, D. Muñoz-Rojas, Mater. Horiz. 2020, advanced article. DOI: 10.1039/D0MH00898B.

[59] S. Sevim, C. Franco, H.J. Liu, H. Roussel, L. Rapenne, J. Rubio-Zuazo, X.Z. Chen, S. Pané, D. Muñoz-Rojas, A.J. DeMello, J. Puigmartí-Luis, Adv. Mater. Technol. 4 (2019) 1800666.

[60] J. Dendooven, K. Devloo-Casier, M. Ide, K. Grandfield, M. Kurttepeli, K.F. Ludwig, S. Bals, P. van der Voort, C. Detavernier, Nanoscale 6 (2014) 14991−14998.

[61] S.P. Sree, J. Dendooven, J. Jammaer, K. Masschaele, D. Deduytsche, J. D'Haen, C.E.A. Kirschhock, J.A. Martens, C. Detavernier, Chem. Mater. 24 (2012) 2775−2780.

[62] J. Dendooven, B. Goris, K. Devloo-Casier, E. Levrau, E. Biermans, M.R. Baklanov, K.F. Ludwig, P. van der Voort, S. Bals, C. Detavernier, Chem. Mater. 24 (2012) 1992−1994.

[63] J.E. Mondloch, W. Bury, D. Fairen-Jimenez, S. Kwon, E.J. DeMarco, M.H. Weston, A.A. Sarjeant, S.T. Nguyen, P.C. Stair, R.Q. Snurr, O.K. Farha, J.T. Hupp, J. Am. Chem. Soc. 135 (2013) 10294−10297.

[64] Y.X. Cui, M. Rimoldi, A.E. Platero-Prats, K.W. Chapman, J.T. Hupp, O.K. Farha, Chem-Euro. J. 10 (2018) 1772−1777.

[65] A. Atilgan, T. Islamoglu, A.J. Howarth, J.T. Hupp, O.K. Farha, ACS Appl. Mater. Inter. 9 (2017) 24555−24560.

[66] M.G. Jeong, D.H. Kim, S.K. Lee, J.H. Lee, S.W. Han, E.J. Park, K.A. Cychosz, M. Thommes, Y.K. Hwang, J.S. Chang, Y.D. Kim, Micropor. Mesopor. Mater. 221 (2016) 101−107.

[67] N.V. Maksimchuk, O.V. Zalomaeva, I.Y. Skobelev, K.A. Kovalenko, V.P. Fedin, O.A. Kholdeeva, Proc. R. Soc. 468 (2012) 2017−2034.

[68] Y.K. Hwang, D.Y. Hong, J.S. Chang, H. Seo, M. Yoon, J. Kim, S.H. Jhung, C. Serre, G. Ferey, Appl. Catal. 358 (2009) 249−253.

[69] J.L. Zhuang, A. Terfort, C. Wöll, Coord. Chem. Rev. 307 (2016) 391−424.

[70] X. Liu, W.T. Fu, E. Bouwman, Chem. Commun. 52 (2016) 6926−6929.

[71] Y. Yoo, Z.P. Lai, H.K. Jeong, Micropor. Mesopor. Mater. 123 (2009) 100−106.

[72] S. Hermes, F. Schroder, R. Chelmowski, C. Wöll, R.A. Fischer, J. Am. Chem. Soc. 127 (2005) 13744−13745.

[73] P. Horcajada, C. Serre, D. Grosso, C. Boissiere, S. Perruchas, C. Sanchez, G. Ferey, Adv. Mater. 21 (2009) 1931−1935.

[74] A. Schoedel, C. Scherb, T. Bein, Angew. Chem. Int. Ed. 49 (2010) 7225−7228.

[75] O. Shekhah, H. Wang, S. Kowarik, F. Schreiber, M. Paulus, M. Tolan, C. Sternemann, F. Evers, D. Zacher, R.A. Fischer, C. Wöll, J. Am. Chem. Soc. 129 (2007) 15118−15119.

[76] M. Kind, C. Wöll, Prog. Surf. Sci. 84 (2009) 230−278.

[77] S. Guthrie, L. Huelsenbeck, A. Salahi, W. Varhue, N. Smith, X. Yu, L.U. Soon, J.J. Choi, N. Swami, G. Giri, Nanoscale Adv. 1 (2019) 2946–2952.

[78] M. Ritala, J. Niinistö, in: A.C. Jones, M.L. Hitchman (Eds.), Chemical Vapour Deposition: Precursors Processes and Applications, The Royal Society of Chemistry, Cambridge, U.K., 2009, pp. 158−206.

[79] I. Stassen, M. Styles, G. Grenci, H. Van Gorp, W. Vanderlinden, S. De Feyter, P. Falcaro, D. De Vos, P. Vereecken, R. Ameloot, Nat. Mater. 15 (2016) 304−310.

[80] Y.J. Zhang, C.H. Chang, Processes 8 (2020) 377.

[81] H. Piri-Moghadam, M.N. Alam, J. Pawliszyn, Anal. Chim. Acta 984 (2017) 42−65.

[82] H.Z. Lan, L.D. Salmi, T. Rönkkö, J. Parshintsev, M. Jussila, K. Hartonen, M. Kemell, M.L. Riekkola, Anal. Chim. Acta 1024 (2018) 93−100.

[83] T. Hatanpaa, M. Ritala, M. Leskela, Coord. Chem. Rev. 257 (2013) 3297−3322.

[84] D.H. Levy, D. Freeman, S.F. Nelson, P.J. Cowdery-Corvan, L.M. Irving, Appl. Phys. Lett. 92 (2008) 192101.

[85] D.H. Levy, Process for atomic layer deposition, US 7,413,982 B2, 2008.

[86] P. Poodt, D.C. Cameron, E. Dickey, S.M. George, V. Kuznetsov, G.N. Parsons, F. Roozeboom, G. Sundaram, A. Vermeer, J. Vac. Sci. Technol. A 30 (2012) 010802.

[87] D. Muñoz-Rojas, Techniques de l'Ingenieur (2016) 1−10.

[88] K. Sharma, R.A. Hall, S.M. George, J. Vac. Sci. Techol. A 33 (2015) 01A132.

[89] D. Muñoz-Rojas, V.H. Nguyen, C.M. de la Huerta, C. Jiménez, D. Bellet. Spatial Atomic Layer Deposition, Chapter: Chemical Vapor Deposition for Nanotechnology, 2019, pp: 1−25, Intech Open.

[90] E. Langereis, S.B.S. Heil, H.C.M. Knoops, W. Keuning, M.C.M. van de Sanden, W.M.M. Kessels, J. Phys. D: Appl. Phys. 42 (2009) 073001.

[91] A.S. Yersak, Y.C. Lee, J.A. Spencer, M.D. Groner, J. Vac. Sci. Techol. A 32 (2014) 01A130.

[92] D.N. Goldstein, J.A. McCormick, S.M. George, J. Phys. Chem. C 112 (2008) 19530−19539.

[93] K. Knapas, A. Rahtu, and M. Ritala, Chem. Vap. Deposition, 15 (2009) 269−273.

[94] K. Knapas, M. Ritala, Crit. Rev. Solid State 38 (2013) 167−202.

[95] B. Rothen-Rutishauser, S. Schürch, P. Gehr, Interaction of particles with membranes. In: Donaldson, K. Borm, P. (Eds.), Particle Toxicology. CRC Press, Boca Raton, 2007, pp. 139−160.

[96] L.L. Ou, B. Song, H.M. Liang, J. Liu, X.L. Feng, B. Deng, T. Sun, L.Q. Shao, Part. Fibre Toxicol. 13 (2016) 57.

[97] M. Ema, M. Gamo, K. Honda, Regul. Toxicol. Pharm. 85 (2017) 7−24.

[98] M. Eddaoudi, J. Kim, N. Rosi, D. Vodak, J. Wachter, M. O'Keeffe, O.M. Yaghi, Science 295 (2002) 469−472.

[99] N.L. Rosi, J. Eckert, M. Eddaoudi, D.T. Vodak, J. Kim, M. O'Keeffe, O.M. Yaghi, Science 300 (2003) 1127−1130.

[100] S. Hermes, M.K. Schroter, R. Schmid, L. Khodeir, M. Muhler, A. Tissler, R.W. Fischer, R.A. Fischer, Angew. Chem. Int. Ed. 44 (2005) 6237−6241.

[101] G. Lu, J.T. Hupp, J. Am. Chem. Soc. 132 (2010) 7832−7833.

[102] Y.S. Li, F.Y. Liang, H.G. Bux, W.S. Yang, J. Caro, J. Membr. Sci. 354 (2010) 48−54.

[103] P. Horcajada, C. Serre, G. Maurin, N.A. Ramsahye, F. Balas, M. Vallet-Regi, M. Sebban, F. Taulelle, G. Ferey, J. Am. Chem. Soc. 130 (2008) 6774−6780.

[104] T. Islamoglu, S. Goswami, Z.Y. Li, A.J. Howarth, O.K. Farha, J.T. Hupp, ACC. Chem. Res. 50 (2017) 805−813.

[105] P. Valvekens, F. Vermoortele, D. De Vos, Catal. Sci. Technol. 3 (2013) 1435−1445.

[106] S.M. Cohen, Chem. Rev. 112 (2012) 970−1000.

[107] K.K. Tanabe, S.M. Cohen, Chem. Soc. Rev. 40 (2011) 498−519.

[108] R.J. Marshall, R.S. Forgan, Eur. J. Inorg. Chem. 2016 (2016) 4310−4331.

[109] S.M. Cohen, J. Am. Chem. Soc. 139 (2017) 2855−2863.

[110] K.B. Klepper, O. Nilsen, P. Hansen, H. Fjellvag, Dalton Trans., 40 (2011) 4636−4646.

[111] V. Bernales, M.A. Ortuño, D.G. Truhlar, C.J. Cramer, L. Gagliardi, ACS Cent. Sci. 4 (2018) 5−19.

[112] P. Deria, J.E. Mondloch, E. Tylianakis, P. Ghosh, W. Bury, R.Q. Snurr, J.T. Hupp, O.K. Farha, J. Am. Chem. Soc. 135 (2013) 16801−16804.

[113] C.T. Lollar, J.S. Qin, J.D. Pang, S. Yuan, B. Becker, H.C. Zhou, Langmuir 34 (2018) 13795−13807.

[114] S.R. Ahrenholtz, C.C. Epley, A.J. Morris, J. Am. Chem. Soc. 136 (2014) 2464−2472.

[115] S. Yuan, Y.P. Chen, J. Qin, W. Lu, X. Wang, Q. Zhang, M. Bosch, T.F. Liu, X. Lian, H.C. Zhou, Angew. Chem., Int. Ed. 54 (2015) 14696−14700.

[116] C. Zhao, X. Dai, T. Yao, W. Chen, X. Wang, J. Wang, J. Yang, S. Wei, Y. Wu, Y. Li, J. Am. Chem. Soc. 139 (2017) 8078−8081.

[117] J.D. Sosa, T.F. Bennett, K.J. Nelms, B.M. Liu, R.C. Tovar, Y.Y. Liu, Crystals 8 (2018) 325.

[118] M.J. Liu, J. Wu, H.W. Hou, Chem-Eur. J. 25 (2019) 2935−2948.

[119] P. Deria, J.E. Mondloch, O. Karagiaridi, W. Bury, J.T. Hupp, O.K. Farha, Chem. Soc. Rev. 43 (2014) 5896−5912.

[120] J.X. Liu, C. Wöll, Chem. Soc. Rev. 46 (2017) 5730−5770.

[121] G.W. Zhan, H.C. Zeng, Chem. Commun. 53 (2017) 72−81.

[122] Y.T. Guntern, J.R. Pankhurst, J. Vávra, M. Mensi, V. Mantella, P. Schouwink, R. Buonsanti, Angew. Chem. Int. Ed. 58 (2019) 12632−12639.

[123] I.S. Kim, J. Borycz, A.E. Platero-Prats, S. Tussupbayev, T.C. Wang, O.K. Farha, J.T. Hupp, L. Gagliardi, K.W. Chapman, C.J. Cramer, A.B.F. Martinson, Chem. Mater. 27 (2015) 4772−4778.

[124] I.S. Kim, Z.Y. Li, J. Zheng, A.E. Platero-Prats, A. Mavrandonakis, S. Pellizzeri, M. Ferrandon, A. Vjunov, L.C. Gallington, T.E. Webber, N.A. Vermeulen, R. Lee Penn, R.B. Getman, C.J. Cramer, K.W. Chapman, D.M. Camaioni, J.L. Fulton, J.A. Lercher, O.K. Farha, J.T. Hupp, A.B.F. Martinson, Chem. Int. Ed. 57 (2018) 909−913.

[125] D. Yang, M.R. Momeni, H. Demir, D.R. Pahls, M. Rimoldi, T.C. Wang, O.K. Farha, J.T. Hupp, C.J. Cramer, B.C. Gates, L. Gagliardi, Faraday Discuss. 201 (2017) 195−206.

[126] A.E. Platero-Prats, A.B. League, V. Bernales, J.Y. Ye, L.C. Gallington, A. Vjunov, N.M. Schweitzer, Z.Y. Li, J. Zheng, B. Layla Mehdi, A.J. Stevens, A. Dohnalkova, M. Balasubramanian, O.K. Farha, J.T. Hupp, N.D. Browning, J.L. Fulton, D.M. Camaioni, J.A. Lercher, D.G. Truhlar, L. Gagliardi, C.J. Cramer, K.W. Chapman, J. Am. Chem. Soc. 139 (2017) 10410−10418.

[127] V. Bernales, M.A. Ortuño, D.G. Truhlar, C.J. Cramer, L. Gagliardi, ACS Cent. Sci. 4 (2018) 5−19.

[128] A.E. Platero-Prats, A. Mavrandonakis, L.C. Gallington, Y.Y. Liu, J.T. Hupp, O.K. Farha, C.J. Cramer, K.W. Chapman, J. Am. Chem. Soc. 138 (2016) 4178−4185.

[129] S. Bhattacharya, W.W. Ayass, D.H. Taffa, A. Schneemann, A.L. Semrau, S. Wannapaiboon, P.J. Altmann, A. Pothig, T. Nisar, T. Balster, N.C. Burtch, V. Wagner, R.A. Fisscher, M. Wark, U. Kortz, J. Am. Chem. Soc. 141 (2019) 3385−3389.

[130] Y.P. He, E.D. Cubuk, M.D. Allendorf, E.J. Reed, J. Phys. Chem. Lett. 9 (2018) 4562−4569.

[131] Bury et al. Metallated metal-organic frameworks. US Patent 9738665 B2, 22 Aug. 2017. & Metalling metal-organic frameworks. US Patent 9562005 B2, 7 Feb. 2017.

[132] A.E. Platero-Prats, Z. Li, L.C. Gallington, A.W. Peters, J.T. Hupp, O.K. Farha, K.W. Chapman, Faraday Discuss. 201 (2017) 337−350.

[133] T.A. Goetjen, X. Zhang, J. Liu, J.T. Hupp, O.K. Farha, ACS Sustain. Chem. Eng. 7 (2019) 2553−2557.

[134] T. Ikuno, J. Zheng, A. Vjunov, M. Sanchez-Sanchez, M. Ortuño, D.R. Pahls, J.L. Fulton, D.M. Camaioni, Z. Li, D. Ray, B.L. Mehdi, N.D. Browning, O.K. Farha, J.T. Hupp, C.J. Cramer, L. Gagliardi, J.A. Lercher, J. Am. Chem. Soc. 139 (2017) 10294−10301.

[135] P. Li, H.D. Zhang, T.C. Wang, T. Duerinck, F.Q. You, J.T. Hupp, O.K. Farha, J.I. Siepmann, R.Q. Snurr, Chem. Mater. 29 (2017) 6315−6328.

[136] C.W. Kung, C.O. Audu, A.W. Peters, H. Noh, O.K. Farha, J.T. Hupp, ACS Energy Lett. 2 (2017) 2394−2401.

[137] A. Sood, P. Sundberg, M. Karppinen, Dalton Trans. 42 (2013) 3869−3875.

[138] A.A. Dameron, D. Seghete, B.B. Burton, S.D. Davidson, A.S. Cavanagh, J.A. Bertrand, S.M. George, Chem. Mater. 20 (2008) 3315−3326.

[139] B.H. Lee, B. Yoon, V.R. Anderson, S.M. George, J. Phys. Chem. C 116 (2012) 3250−3257.

[140] X. Liang, A.W. Weimer, Curr. Opin. Solid State Mater. Sci. 19 (2015) 115−125.

[141] K. Van de Kerckhove, M.K.S. Barr, L. Santinacci, P.M. Vereecken, J. Dendooven, C. Detavernier, Dalt. Trans. 47 (2018) 5860−5870.

[142] P. Sundberg, M. Karppinen, Beilstein J. Nanotechnol. 5 (2014) 1104−1136.

[143] Z. Gao, Y. Qin, Acc. Chem. Res. 50 (2017) 2309−2316.

[144] M. Rimoldi, V. Bernales, J. Borycz, A. Vjunov, L.C. Gallington, A.E. Platero-Prats, I.S. Kim, J.L. Fulton, A.B.F. Martinson, J.A. Lercher, K.W. Chapman, C.J. Cramer, L. Gagliardi, J.T. Hupp, O.K. Farha, Chem. Mater. 29 (2017) 1058−1068.

[145] A.W. Peters, Z.Y. Li, O.K. Farha, J.T. Hupp, ACS Appl. Mater. Inter. 8 (2016) 20675−20681.

[146] R.C. Klet, T.C. Wang, L.E. Fernandez, D.G. Truhlar, J.T. Hupp, O.K. Farha, Chem. Mater. 28 (2016) 1213−1219.

[147] R.H. Palmer, C.-W. Kung, J. Liu, O.K. Farha, J.T. Hupp, Langmuir 34 (2018) 14143−14150.

[148] M. Rimoldi, J.T. Hupp, O.K. Farha, ACS Appl. Mater. Inter. 9 (2017) 35067−35074.

[149] A.W. Peters, Z.Y. Li, O.K. Farha, J.T. Hupp, ACS Nano 9 (2015) 8484−8490.

[150] Z.Y. Li, A.W. Peters, J. Liu, X. Zhang, N.M. Schweitzer, J.T. Hupp, O.K. Farha, Inorg. Chem. Front. 4 (2017) 820−824.

[151] S. Ahn, N.E. Thornburg, Z.Y. Li, T.C. Wang, L.C. Gallington, K.W. Chapman, J.M. Notestein, J.T. Hupp, O.K. Farha, Inorg. Chem. 55 (2016) 11954−11961.

[152] M. Rimoldi, L.C. Gallington, K.W. Chapman, K. MacRenaris, J.T. Hupp, O.K. Farha, Chem. Eur. J. 23 (2017) 8532−8536.

[153] C.W. Kung, J.E. Mondloch, T.C. Wang, W. Bury, W. Hoffeditz, B.M. Klahr, R.C. Klet, M.J. Pellin, O.K. Farha, J.T. Hupp, ACS Appl. Mater. Inter. 7 (2015) 28223−28230.

[154] H. Noh, Y.X. Cui, A.W. Peters, D.R. Pahls, M.A. Ortuño, N.A. Vermeulen, C.J. Cramer, L.Gagliardi, J.T. Hupp, O.K. Farha, J. Am. Chem. Soc. 138 (2016) 14720−14726.

[155] S.M.J. Rogge, A. Bavykina, J. Hajek, H. Garcia, A.I. Olivos-Suarez, A. Sepúlveda-Escribano, A. Vimont, G. Clet, P. Bazin, F. Kapteijn, M. Daturi, E.V. Ramos-Fernandez, F.X. Llabrés i Xamena, V. Van Speybroeck, J. Gascon, Chem. Soc. Rev. 46 (2017) 3134−3184.

[156] L. Jiao, Y. Wang, H.L. Jiang, Q. Xu, Adv. Mater. 30 (2018) 1703663.

[157] A. Kirchon, L. Feng, H.F. Drake, E.A. Joseph, H.C. Zhou, Chem. Soc. Rev. 47 (2018) 8611−8638.

[158] K. Manna, P. Ji, F.X. Greene, W. Lin, J. Am. Chem. Soc., 138 (2016) 7488−7491.

[159] Z.Y. Li, N.M. Schweitzer, A.B. League, V. Bernales, A.W. Peters, A. “Bean” Getsoian, T.C. Wang, J.T. Miller, A. Vjunov, J.L. Fulton, J.A. Lercher, C.J. Cramer, L. Gagliardi, J.T. Hupp, O.K. Farha, J. Am. Chem. Soc. 138 (2016) 1977−1982.

[160] K. Manna, P. Ji, Z. Lin, F.X. Greene, A. Urban, N.C. Thacker, W. Lin, Nat. Commun. 7 (2016) 12610.

[161] P. Ji, K. Manna, Z. Lin, A. Urban, F.X. Greene, G. Lan, W. Lin, J. Am. Chem. Soc. 138 (2016) 12234.

[162] A.J.M. Mackus, N.F.W. Thissen, J.J.L. Mulders, P.H.F. Trompenaars, M.A. Verheijen, A.A. Bol, W.M.M. Kessels, J. Phys. Chem. C 117 (2013) 10788−10798.

[163] J. Hämäläinen, M. Ritala, M.Leskela, Chem. Mater. 26 (2014) 786−801.

[164] J.S. King, A. Wittstock, J. Biener, S.O. Kucheyev, Y.M. Wang, T.F. Baumann, S.K. Giri, A.V. Hamza, M. Baeumer, S.F. Bent, Nano Lett. 8 (2008) 2405−2409.

[165] T.D. Gould, A.M. Lubers, A.R. Corpuz, A.W. Weimer, J.L. Falconer, J.W. Medlin, ACS Catal. 5 (2015) 1344−1352.

[166] A. Goulas, J.R. van Ommen, J. Mater. Chem. A 1 (2013) 4647−4650.

[167] J.A. Enterkin, W. Setthapun, J.W. Elam, S.T. Christensen, F.A. Rabuffetti, L.D. Marks, P.C. Stair, K.R. Poeppelmeier, C.L. Marshall, ACS Catal. 1 (2011) 629−635.

[168] Y. Zhou, D.M. King, X.H. Liang, J.H. Li, A.W. Weimer, Appl. Catal. B 101 (2010) 54−60.

[169] J.H. Li, X.H. Liang, D.M. King, Y.B. Jiang, A.W. Weimer, Appl. Catal. B 97 (2010) 220−226.

[170] S. Peng, M. Li, X.X. Yang, P.H. Li, H. Liu, W. Xiong, X.Y. Peng, Ceram. Int. 45 (2019) 18128−18134.

[171] M. Wber, M. Bechelany, Pure Appl. Chem. 92 (2019) 213−222.

[172] K. Leus, J. Dendooven, N. Tahir, R.K. Ramachandran, M. Meledina, S. Turner, G. Van Tendeloo, J.L. Goeman, J. Van der Eycken, C. Detavernier, P. Van Der Voort, Nanomaterials 6 (2016) 45.

[173] K. Leus, C. Krishnaraj, L. Verhoeven, V. Cremers, J. Dendooven, R.K. Ramachandran, P. Dubruel, P. Van Der Voort, J. Catalysis, 360 (2018) 81−88.

[174] P.C. Lemaire, D.T. Lee, J.J. Zhao, G.N. Parsons, ACS Appl. Mater. Inter. 9 (2017) 22042−22054.

[175] A. Sood, P. Sundberg, M. Karppinen, Dalton Trans. 42 (2013) 3869−3875.

[176] C. Boehler, F. Güder, U.M. Kücükbayrak, M. Zacharias, M. Asplund, Sci. Rep. 6 (2016) 19574.

[177] L.D. Salmi, M.J. Heikkilä, E. Puukilainen, T. Sajavaara, D. Grosso, M. Ritala. Micropor. Mesopor. Mater. 182 (2013) 147−154.

[178] L.D. Salmi, M.J. Heikkilä, M. Vehkamäki, E. Puukilainen, M. Ritala, J. Vac. Sci. Tech. A. 33 (2015) 01A121.

[179] E. Ahvenniemi, M. Karppinen, Chem. Commun. 52 (2016) 1139–1142.

[180] K. B. Lausund, V. Petrovica, O. Nilsen, Dalton Trans. 46 (2017) 16983–16992.

[181] Y.L. Hu, J. Liao, D.M. Wang, G.K. Li, Anal. Chem. 86 (2014) 3955–3963.

[182] H.L. Jiang, B. Liu, T. Akita, M. Haruta, H. Sakurai, Q. Xu, J. Am. Chem. Soc. 131 (2009) 11302–11303.

[183] D. Esken, S. Turner, O. I. Lebedev, G.V. Tendeloo, R.A. Fischer, Chem. Mater. 22 (2010) 6393–6401.

[184] K. Sugikawa, Y. Furukawa, K. Sada, Chem. Mater. 23 (2011) 3132–3134.

[185] J.Y. Zeng, M.K. Zhang, M.Y. Peng, D. Gong, X.Z. Zhang, Adv. Funct. Mater. 28 (2018) 1705451.

[186] Y.B. Zhao, N. Kornienko, Z. Liu, C.H. Zhu, S. Asahina, T.R. Kuo, W. Bao, C.L. Xie, A. Hexemer, O. Terasaki, P.D. Yang, O.M. Yaghi, J. Am. Chem. Soc. 137 (2015) 2199−2202.

[187] K. Vellingiri, L. Philip, K.H. Kim, Coord. Chem. Rev. 353 (2017) 159−179

[188] S.M. George, B. Yoon, A.A. Dameron, ACC Chem. Res. 42 (2009) 498−508.

[189] J. Zhao, B. Gong, W.T. Nunn, P.C. Lemaire, E.C. Stevens, F.I. Sidi, P.S. Williams, C.J. Oldham, H.J. Walls, S.D. Shepherd, M.A. Browe, G.W. Peterson, M.D. Losego, G.N. Parsons, J. Mater. Chem. A 3 (2015) 1458−1464.

[190] S.E. Hankari, M. Bousmina, A.E. Kadib, Prog. Mater. Sci. 106 (2019) 100579.

[191] J.J. Zhao, W.T. Nunn, P.C. Lemaire, Y.L. Lin, M.D. Dickey, C.J. Oldham, H.J. Walls, G.W. Peterson, M.D. Losego, G.N. Parsons, J. Am. Chem. Soc. 137 (2015) 13756−13759.

[192] M.T. Zhao, Y. Huang, Y.W. Peng, Z.Q. Huang, Q.L. Ma, H. Zhang, Chem. Soc. Rev. 47 (2018) 6267−6295.

[193] N. Kornienko, Y.B. Zhao, C.S. Kley, C.H. Zhu, D. Kim, S. Lin, C.J. Chang, O.M. Yaghi, P.D. Yang, J. Am. Chem. Soc. 137 (2015) 14129−14135.

[194] S. Hermes, D. Zacher, A. Baunemann, C. Wöll, R.A. Fischer, Chem. Mater. 19 (2007) 2168−2172.

[195] Y. Yoo, H.K. Jeong, Chem. Commun. 2008, 2441−2443.

[196] D. Zacher, O. Shekhah, C. Wöll, R.A. Fischer, Chem. Soc. Rev. 38 (2009) 1418−1429.

[197] N. Kornienko, Y. Zhao, C.S. Kley, C. Zhu, D. Kim, S. Lin, C.J. Chang, O.M. Yaghi, P. Yang, J. Am. Chem. Soc. 137 (2015) 14129−14135.

[198] R. Wang, F. Kapteijn, J. Gascon, Asian J. 14 (2019) 3452−3461.

[199] J. Zhao, M.D. Losego, P.C. Lemaire, P.S. Williams, B. Gong, S.E. Atanasov, T.M. Blevins, C.J. Oldham, H.J. Walls, S.D. Shepherd, M.A. Browe, G.W. Peterson, G.N. Parsons, Adv. Mater. Interf. 1 (2014) 1400040.

[200] S. Lawson, A.A. Rownaghi, F. Rezaei, Energy Technol. 6 (2018) 694−701.

[201] J. Zhao, D.T. Lee, R.W. Yaga, M.G. Hall, H.F. Barton, I.R. Woodward, C.J. Oldham, H.J. Walls, G.W. Peterson, G.N. Parsons, Angew. Chem. Int. Ed. 55 (2016) 13224−13228.

[202] P.C. Lemaire, J.J. Zhao, P.S. Williams, H.J. Walls, S.D. Shepherd, M.D. Losego, G.W. Peterson, G.N. Parsons, ACS Appl. Mater. Inter. 8 (2016) 9514−9522.

[203] D.T. Lee, J.J. Zhao, G.W. Peterson, G.N. Parsons, Chem. Mater. 29 (2017) 4894−4903.

[204] D.T. Lee, J.J. Zhao, C.J. Oldham, G.W. Peterson, G.N. Parsons, ACS Appl. Mater. Inter. 9 (2017) 44847−44855.

[205] D.B. Dwyer, D. Lee, S. Boyer, W.E. Bernier, G.N. Parsons, Jr. W.E. Jones, ACS Appl. Mater. Inter. 10 (2018) 25794−25803.

[206] D.T. Lee, J.D. Jamir, G.W. Peterson, G.N. Parsons, Small 15 (2019) 180513.

[207] H.F. Barton, A.K. Davis, G.N. Parsons, ACS Appl. Mater. Inter. 12 (2020) 14690−14701.

[208] K. Tan, S. Jensen, L. Feng, H. Wang, S. Yuan, M. Ferreri, J.P. Klesko, R. Rahman, J. Cure, J. Li, H.-C. Zhou, T. Thonhauser, Y.J. Chabal, Chem. Mater. 31 (2019) 2286−2295.

[209] L.C. Gallington, I.S. Kim, W.-G. Liu, A.A. Yakovenko, A.E. Platero-Prats, Z.Y. Li, T.C. Wang, J.T. Hupp, O.K. Farha, D.G. Truhlar, A.B.F. Martinson, K.W. Chapman, J. Am. Chem. Soc. 138 (2016) 13513−13516.

[210] W.G. Liu, D.G. Truhlar, Chem. Mater. 29 (2017) 8073−8081.